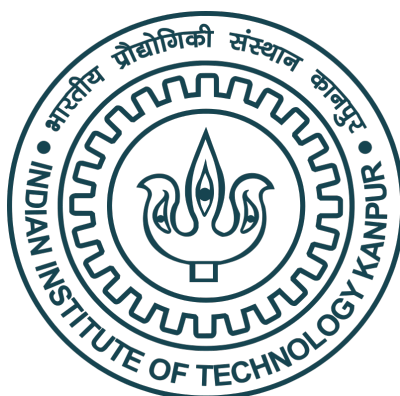


Towards Fast, Flexible and Sensor-Free Control of Standalone PVDG Systems

A Thesis Submitted
in Partial Fulfillment of the Requirements
for the Degree of
Master of Technology

by
Meher Preetam Korukonda
(12104172)



to the
Department of Electrical Engineering
INDIAN INSTITUTE OF TECHNOLOGY KANPUR
Kanpur, INDIA - 208016
June, 2020

Certificate

This is to certify that the work contained in the thesis entitled “**Towards Fast, Flexible and Sensor-Free Control of Standalone PVDG Systems**”, by Meher Preetam Korukonda (Roll No.12104172), has been carried out under our supervision for the partial fulfillment of M.Tech degree in the Department of Electrical Engineering, IIT Kanpur and this work has not been submitted elsewhere for any other degree.



Laxmidhar Behera

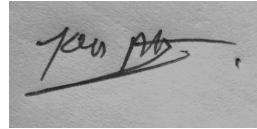
Professor

Department of Electrical Engineering
Indian Institute of Technology Kanpur
Kanpur, INDIA - 208016

June, 2020

DECLARATION

This is to certify that the thesis titled *Towards Fast, Flexible and Sensor-Free Control of Standalone PVDG Systems* has been authored by me. It presents the research conducted by me under the supervision of Prof. Laxmidhar Behera. To the best of my knowledge, it is an original work, both in terms of research content and narrative, and has not been submitted elsewhere, in part or in full, for a degree. Further, due credit has been attributed to the relevant state-of-the-art and collaborations (if any) with appropriate citations and acknowledgments, in line with established norms and practices.



Signature

Name : Meher Preetam Korukonda

Programme: MTech

Department: Electrical Engineering

Indian Institute of Technology Kanpur,

Kanpur-208016, India

ABSTRACT

Name of Student: Meher Preetam Korukonda Roll no.: 12104172
Degree for which submitted: M.Tech Department: Electrical Engineering
Title: Towards Fast, Flexible and Sensor-Free Control of Standalone PVDG Systems.
Name of Thesis Supervisor: Prof. Laxmidhar Behera
Month and year of Thesis submission: May, 2020.

In this thesis, the problem of fast, effective and low cost control of a Standalone Photovoltaic Distributed Generation (SPVDG) system is considered. On-site generation from these systems is more efficient when the power is transmitted via DC due to elimination of transmission losses and needless energy conversions. The inherent low-inertia of these systems added with fluctuation of output power and uncertain load consumption, calls for advanced control techniques to ensure fast and stable operation during various intermittencies. These techniques are expensive since they demand installation of many sophisticated sensors. The computation power provided by the fast growing IC technology can be utilized to estimate different parameters in a system and reduce the need for expensive sensing equipment. This work provides solutions to problems encountered in the development of faster, more stable and sensor-free voltage control and maximum power point tracking(MPPT) for SPVDG systems with PV and battery.

First, a model based MPPT technique fitted with a Newton-Raphson based temperature and irradiation estimation scheme is proposed for faster tracking and higher PV power extraction. Next, a unified direct perturbation based control algorithm is proposed which carries out both MPPT and DC bus voltage control simultaneously using voltage measurements only from the load side. Although this technique cuts down the overall cost, it suffers from poor performance in wake of large disturbances. To improve the speed and operating range of the SPVDG, a nonlinear back-stepping based control strategy is proposed which tackles various intermittencies in weather, load and battery voltage. However, this controller again suffers from higher cost as many parameters of the DCMG unit need to be explicitly measured. Hence, in the final part of the thesis, the back-stepping based controller design is revisited with inclusion of disturbance observers for grid voltage control. These observers estimate unknown parameters like load and battery voltage and eliminate additional measurements. It can be seen that adoption of the techniques proposed in this thesis contributes towards faster, sensor-free control of the DCMG for a greater range of operating conditions.

Acknowledgements

Firstly, I would like to express my heartfelt gratitude to my guide, Prof. L. Behera for his valuable guidance and support throughout my work. He has provided with immense opportunities to explore and collaborate which finally took the form of this thesis. Apart from being a visionary, he has inspired me with the right mix of strictness and compassion to ensure my development in all walks of life.

I wish to express my gratitude to the Bhaktivedanta Club where I was introduced teachings of H.D.G. A. C. Bhaktivedanta Swami Prabhupada and my spiritual master. I am highly obliged to all the devotees, in particular Mrs. Gopali, Dr.Vipul, Dr.V.Sudheendhra, Dr.Akhaya Nayak, Dr.Himanshu , Mr.Ashish Gupta, Dr. Jayant and Mr. Devaki Nandan for guiding me through practical issues in life. I am especially grateful to Mr.Tharun Reddy, Mr.Ravi Prakash, Dr.Nitesh, Vinay Gupta, Jitendra Soni, Sachin Sahoo, Praful, Hariom and Jivnesh who readily took up many responsibilities to help me focus on my research. I wish to express my heartfelt thanks to Mr. Akshay Samal, Amruta, Sunil Dutta, Bharti, Sandeep Gupta, Prem Raj, Mrs. Swati Gupta, Mrs.Sujata Samal and Mrs. Chitra whose loving association inspires me to be a better person.

I would like to express my deep gratitude to the esteemed faculty members of IIT Kanpur, who ignited within me, a deep sense of appreciation for engineering. Especially, I would like to thank Prof. P.Sensarma, Prof. Santanu Mishra, Prof. S.C.Srivastav, Prof. S.P. Das, and Prof. R. Potluri who taught me the basics of power electronics, power systems and control.

I am highly grateful to our lab in-charges Abhay ji, Uday ji, Kamlesh ji, and assistant Harishankarji for their support. I wish to thank Dr.Manmohan, Mr. Amir,Mr.Swaroop Mishra, Mr. Manoranjan, Dr.Narendra Dhar and Mr.Shamim for the stimulating discussions on microgrids. I would specially like to thank all my labmates: Ashish, Archit, Anuj, Vibhu, Padmini, Radheshyam, Subhash and especially my seniors Dr.Prem, Dr.Felix, Dr.Awhan, Dr. Samrat, Dr. Ranjith and Dr. Anima for extending me all help whenever I needed it.

Most importantly, I would like to thank my parents, and my brother for their placing their faith in me, encouraging me in challenging times while tolerating all the inconveniences I have put through them with love and patience.

Contents

Acknowledgements	iv
List of Figures	viii
List of Tables	ix
1 Introduction	1
1.1 Motivation	1
1.2 System Overview	2
1.3 Thesis Organization	3
1.4 Thesis Contributions	4
2 Fast Model-based MPPT for PV Arrays with Temperature and Irradiation Estimation	5
2.1 Introduction	5
2.2 Mathematical Modeling of the PV Array	7
2.2.1 PV characteristic	8
2.2.2 Power Converter	10
2.3 Temperature and Irradiance Detection	10
2.4 Calculation of desired states	12
2.5 Simulation Results and Discussion	14
2.6 Summary	16
3 A Unified Sensor-free Control Strategy for MPPT and Voltage Control in Standalone PVDG Systems	18
3.1 Introduction	18
3.2 Configuration Of the SPVDG	19
3.3 Unified Sensorless Control Strategy	21
3.3.1 Direct perturbation based sensor-free MPP tracking	22
3.3.2 Automatic battery charging/discharging with seamless mode transition for DC grid voltage control	24
3.4 Simulation Results	25

3.5	Summary	27
4	A Nonlinear Back-stepping based Controller for Standalone PVDG Systems	28
4.1	Introduction	28
4.2	System Description and Modeling	29
4.2.1	Basic Blocks	29
4.2.2	Hierarchical Control Structure	30
4.2.3	State Space Model	30
4.3	Reference Generation:	32
4.4	Backstepping based Nonlinear Controller Design	33
4.4.1	Controller Design Procedure:	33
4.5	Results	35
4.5.1	Case-1: Variation in Irradiance	36
4.5.2	Case-2: Variation in Temperature	37
4.5.3	Case-3: Variation in Load	37
4.6	Summary	39
5	Disturbance Observer based Backstepping Controller for the Isolated DCMG Unit	40
5.1	Introduction	40
5.2	Disturbance Observer Based Back-stepping Controller Design	42
5.3	Simulation Results	44
5.3.1	Case-1: Change in Irradiance	45
5.3.2	Case-2: Change in Temperature	45
5.3.3	Case-3: Change in Load	47
5.4	Summary	48
6	Conclusion and Future Scope	51
6.1	Conclusion	51
6.2	Future Scope	52
	List of Publications	53
	Bibliography	54
	Index	63

List of Figures

1.1	Structure of SPVDG System	3
2.1	Equivalent circuit of (a) Single PV cell (b) Complete PV array	9
2.2	Effect of series and shunt resistance of P-V curve for different temperature and irradiance.	9
2.3	PV Array in conjunction with dc-dc boost converter.	10
2.4	Different cases of variation in temperature and irradiance	15
2.5	Comparison of estimated temperature with actual value	15
2.6	Comparison of estimated irradiance with actual value	16
2.7	Desired voltage, estimated voltage and actual current for MPP under different environmental conditions.	16
2.8	Desired Power, estimated power and actual power for MPP under different environmental conditions.	17
2.9	Desired, calculated and actual inductor current at MPP for different environmental conditions	17
2.10	PV voltage, power and duty ratio for different load conditions	17
3.1	Overall schematic of the standalone DC microgrid.	20
3.2	Equivalent circuit of (a) single PV cell (b) PV array.	20
3.3	Control strategy for MPPT and DC bus voltage control	22
3.4	PV power variation due to change in solar irradiance	25
3.5	Inductor current associated with BESS	26
3.6	Duty ratio of buck and boost operation	26
3.7	DC bus voltage	27
4.1	Structure of SPVDG System	30
4.2	Power Architecture of the SPVDG System	31
4.3	Case-1: PV states	36
4.4	Case-1: Battery States	37
4.5	Case-2: PV states	38
4.6	Case-2: Battery States	38
4.7	Case-3: PV states	39

4.8	Case-3: Battery States	39
5.1	Structure of SPVDG System with observer	40
5.2	Case-1: Relevant states	46
5.3	Case-1: Observer values	47
5.4	Case-2: Relevant states	48
5.5	Case-2: Observer values	49
5.6	Case-3: Relevant states	49
5.7	Case-3: Observer values	50

List of Tables

2.1	Desired values of PV voltage, Current and Power for different environmental conditions	13
2.2	parameters used for simulation and hardware implementation	15
3.1	Parameter Specification	21
3.2	Set of conditions for buck operation	23
3.3	Set of conditions for boost operation	24
4.1	Parameter Specification	36
5.1	Parameter Specification	45

Chapter 1

Introduction

1.1 Motivation

Renewable energy is penetrating the power generation sector today like never before. Especially, solar PVDG systems are gaining popularity due to a continuous reduction in the cost of solar panel, efficiency improvement, advancement in power electronics, and, ambitious goals set by different countries to deploy PV sources into the existing electrical network [1]. Certain PVDG configurations, like the ones used in solar home projects in Africa (e.g., Kenya) [2], are seen to provide high-quality power to remote areas in a convenient and practical manner due to which many inaccessible areas gained access to cheap and reliable electricity supply.

PVDG systems can be categorized into two types, a) stand-alone system and b) grid connected system. The standalone PVDG system (SPVDG) [3] is used in two different configurations, namely, with and without storage. In the SPVDG system without storage, the extracted power is directly supplied to the load. In case of an SPVDG system with storage, the extracted power from PV is used both for feeding the load and charging the battery [4] as well. An overview of the SPVDG system structure shown in Fig. 5.1.

Of late, deployment of DC based SPVDG systems and microgrids has gone upward since PVDG systems and many other renewable sources directly generate DC output power which can directly be connected to DC loads [5]. If loads are supplied directly with DC power, the efficiency of the system becomes higher due to the reduction of conversion losses from sources to loads. Apart from these, DC implementation of SPVDG systems can also overcome some limitations associated with AC such as frequency synchronization, control of reactive power flow, and power quality problems [6]. However, the characteristics of PV arrays are highly intermittent and so are the loading conditions in an SPVDG system and this makes control of these systems quite difficult [7]. Storage can be used to eliminate the

fluctuations in microgrids by storing or releasing energy [8] using bidirectional DCDC converters along with appropriate tuning of control parameters.

For a standalone PV system with storage, maximum power point tracking and DC bus voltage regulation constitute the major control problems to be dealt with. While MPPT ensures that maximum power is extracted from the PV array at any give time, DC bus voltage control indicates the overall power balance in the system. Research in the field of SPVDG has diversified into many areas such as power electronic converter architecture [9], maximum-power-point tracking (MPPT) [10], battery life expansion [11], efficiency improvement [12], power flow management of microgrids [13], communication design [14] and distributed control [15–19]. On the control side, many controllers have been designed for these systems including fractional PID [20], and phase angle control [21] apart from classical control techniques.

It has been noticed from all the above literature that model based nonlinear control techniques work much better when we need robust performance in MPPT and voltage control over large range of operating conditions. However, these techniques require many sophisticated sensors compared to conventional techniques which naturally increase the overall cost of the system. Hence, in this thesis, we use many computation based techniques to overcome some of the issues in this direction and provide better control solutions for the SPVDG system.

1.2 System Overview

The SPVDG system under consideration consists of a PV array and a battery energy storage system (BESS) feeding to a load. The PV array continuously extracts power from the available solar energy and transfers it to the load using a DC-DC converter as shown in Fig. 4.2. The BESS is connected to the grid via a bidirectional DC-DC converter. This is essential to modulate power flow in both the directions as demanded by load conditions in the SPVDG system. Both the converters are controlled to regulate the desired flow of power in the PVDG system.

As evident from Fig.1.1, the hierarchy of control in the SPVDG system is present in two levels of the SPVDG system namely, primary and secondary. The secondary level controller handles the overall energy management function of the SPVDG. It is responsible for ensuring maximum power extraction from the PV panel and also plan the power flow of the battery depending on the imbalance between the PV power generation and load consumption. The secondary controller achieves this operation by setting the reference values for all the important states in the SPVDG system like inductor currents and capacitor voltages. The major function of the primary controller is to bring the system states to the reference values set by the secondary controller. A properly designed primary controller performs this function even in

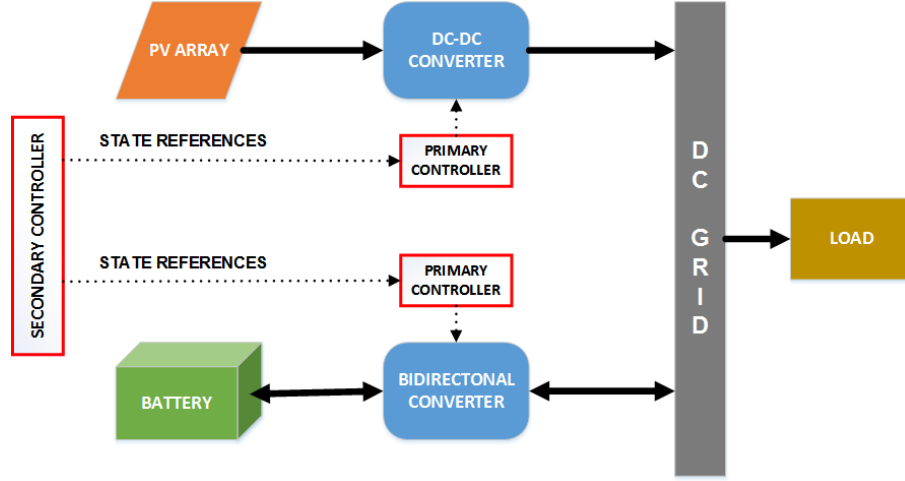


Figure 1.1: Structure of SPVDG System

the presence of large disturbances affecting the system time to time.

1.3 Thesis Organization

The major objective of this thesis is to provide computation based solutions to reduce sensor requirement in advanced model based control techniques for the SPVDG system. Every chapter takes a step forward in this direction and finally culminates into development of nonlinear control techniques with observers to reduce sensors.

The chapter-wise descriptions of the work done in this thesis is given as follows:

Chapter 2 portrays the development of a temperature and irradiance estimation technique that obviates irradiation and temperature sensors in high performance model based MPPT control techniques.

Chapter 3 describes a thrifty and unified control strategy for MPPT and voltage control which is very simple to implement and requires no sensors to be placed on the PV panel.

Chapter 4 delineates a back-stepping based nonlinear control technique which directly uses the large signal model of the SPVDG and provides an extended range of operation along with faster performance.

Chapter 5 incorporates the concept of disturbance observer into the back-stepping control strategy developed in Chapter 4 to reduce the number of sensors used while preserving the benefits of using a nonlinear control scheme.

Chapter 6 concludes the thesis with some observations and indicates the future scope of work to be carried out.

1.4 Thesis Contributions

The major contributions of this thesis can be summarized as follows:

- For the first time, Newton-Raphson technique has been applied to estimate the PV array curve with only two operating points.
- An online technique for estimation of temperature and irradiation considering non-idealities in PV model was developed.
- An integrated algorithm is developed which exploits the natural electrical interconnection between both the PV and battery subsystems to achieve both MPPT and ancillary service like voltage control in a concomitant manner. This method is very simple with negligible computational burden and carries out two functions in a single control module. It is a low cost method as it uses less sensors.
- Reduction in transient time while regulating the DC voltage and achieving MPPT of SPVDG system through incorporation of back-stepping based control. The major takeaway from this concept is the manner in which the entire system model was fragmented inorder to successfully apply the nonlinear technique.
- A disturbance observer was incorporated to estimate different parameters in the SPVDG system to reduce sensors and facilitate the back-stepping based control.

Chapter 2

Fast Model-based MPPT for PV Arrays with Temperature and Irradiation Estimation

In this chapter, an algorithm is proposed to achieve maximum power point tracking in a single step under fast varying environmental and load conditions. First, the ambient irradiation and temperature values are estimated using Newton-Raphson (NR) method. Then, the reference PV voltage and current for the corresponding MPP is calculated.

2.1 Introduction

In the present day scenario, solar photovoltaic energy is considered as a viable alternative to the conventional energy sources such as thermal, gas, nuclear, etc. Therefore, research is being carried out on various issues related to electric power generation for different applications using photovoltaic (PV) energy sources [22–25]. PV energy system has several advantages such as pollution-free, abundant availability, less maintenance and near zero carbon emission. However, the non linear current voltage (I-V) characteristic of PV arrays makes it necessary to operate at MPP in order to extract maximum power from it. There are many MPPT algorithms reported in the literature [26–28]. Efficient MPPT algorithms should impel PV systems to harvest maximum power available irrespective of the change in atmospheric condition or load. The popular MPPT algorithms are mainly based on different techniques like perturb and observe (P&O) [29] [30], incremental conductance (INC) [31] [32], hill climbing, fractional open-circuit voltage [33], fractional short-circuit current [34], ripple correlation control [35], fuzzy logic control [36], [37], particle swarm optimization [38], [39], artificial neural network [40], genetic algorithm [41]. These algorithms

differ from one another based on their ease of implementation, tracking speed, number of sensors used, tracking efficiency, cost, etc. The P&O MPPT technique is quite straight forward in computation and can easily be implemented using any low-cost microcontroller. However, in steady-state, the output power oscillates around the MPP resulting in inefficient extraction of available power [30]. These power oscillations can be minimized by reducing the voltage step size, but it takes more time to reach the MPP. Moreover, during rapid change in environmental conditions, there is a possibility that the operating point of PV system may deviate from MPP [42].

In [43], a variable step INC method (VSINC) was proposed where the voltage step size is adaptively varied based on the rate of change of power with voltage. Even then, as the operating point reaches MPP, the step size reduces to a smaller value which requires more time to converge. However, in this technique also, settling time to reach MPP is high because the voltage step size is reduced to a smaller value as the operating point reached near MPP. Further, a fast converging MPPT (FC-MPPT) method was proposed in [44] which quickly shifts the operating point near to MPP region using geometric techniques and then applies incremental conductance to reach the actual MPP. However, in case of fast varying environmental and load conditions, this method does not perform well because the obtained approximate operating points tend to be quite far from MPP region as there is no information of the system model being used. The MPPT methods discussed so far gradually arrive at MPP by varying the reference voltage/current values based on certain search criteria. They search for MPP in each step without actually possessing the information about complete characteristics of PV system. Alternatively, many model based MPPT techniques have been proposed in literature [45]- [46]. These techniques capture the complete range of I-V relationship using different models and directly find the MPP using computational means. The PV system is then directly controlled to operate at MPP. Various model estimation techniques using artificial neural networks (ANN) [45] and neuro-fuzzy models [47] were proposed for this purpose. While these techniques find the MPPs accurately, they often suffer from heavy computational burden. Moreover, if there are unprecedented changes in environmental and physical conditions, these models need to be retrained to accurately reflect the changes. On the other hand, physical model estimation techniques using curve-fitting methods have also shown much presence in the recent literature. These techniques solve the different electrical models of the solar cell such as single-diode model [48], double diode-model [49] under controlled conditions and extrapolate them for other working conditions and find the MPP using numerical techniques. Many of these resort to [50], analytical five point method [51] or heuristic techniques like PSO [52] to arrive at the accurate characteristics of the solar cell. An analytical expression was also developed for the direct determination of MPP references

using Lambert W function [46]. However, in these model estimation based MPPT methods, additional hardware is required for measuring temperature and irradiance which adds to cost of the overall system.

To eliminate the need of temperature and irradiation sensors, many methods has been developed to estimate the temperature and irradiance and improve detection of the MPP. For instance, [53] proposed a combined model based and heuristic MPPT (CMH-MPPT) which works similar to FC-MPPT method by forcing the operating point to a near MPP zone. However, its performance is superior to that of FC-MPPT during rapid change in environmental conditions due to the additional model based temperature estimation feature included. The limitation of this method is that it cannot reach MPP in a single step. On the contrary, [54] proposed a single-step formula for finding MPP using simplified polynomial analytical model which estimates its parameters in real time without using additional environmental sensors. However, its single-step formula necessitates placement of an additional voltage sensor at the output. It is also observed that in most of these works, the non-idealities of PV models have been neglected for simplicity. To the best of the authors' knowledge, there is no work in the literature to find MPP for fast varying environmental and load conditions in a single step using only voltage and current sensors while considering PV array non-idealities.

In this chapter, an algorithm is proposed to achieve maximum power point tracking in a single step under fast varying environmental and load conditions. First, the ambient irradiation and temperature values are estimated using Newton-Raphson (NR) method. Then, the reference PV voltage and current for the corresponding MPP is calculated.

The following is the organization of this chapter. Section 2.2 elucidates the mathematical modeling of a PV array and PV array characteristics. Section 2.3 discusses the temperature and irradiation technique proposed in this chapter using only two operating points on the curve. Section 2.4 shows how to obtain the desired values of all the states present in the PV array system. Section 2.5 shows the estimation results that are obtained in different temperature and irradiation conditions and also in different loading conditions while Section 2.6 summarizes the entire technique and its application.

2.2 Mathematical Modeling of the PV Array

The basic PV system configuration and its mathematical description is presented in the following subsections:

2.2.1 PV characteristic

The electrical characteristics of a PV cell are usually described by the single-diode model with acceptable accuracy [55]. The equivalent circuit of a single PV cell using single-diode model is shown in Fig.2.1(a). In practice, PV cells are combined in series and parallel to form a large PV array. The equivalent circuit of a PV array consisting of n_s series and n_p parallel PV cells is shown in Fig.2.1(b). The current-voltage relationship of the PV array is given by [56]

$$i_{pv} = n_p I_g - n_p I_s \left(e^{\frac{q(v_{pv} + i_{pv} R_s)}{n_s p K T}} - 1 \right) - \frac{v_{pv} + i_{pv} R_s}{R_{sh}} \quad (2.1)$$

where

I_g : Photogenerated current of a single PV cell

i_{pv} : Output current of the PV array

v_{pv} : Output voltage of the PV array

I_s : Reverse saturation current of diode

r_s : Series resistance of a single cell

r_{sh} : Parallel resistance of a single cell

n_s : Numbers of series cells in PV array

n_p : Numbers of parallel cells in PV array

R_s : Series resistance of PV array

R_{sh} : Parallel resistance of PV array

p : Diode ideality constant

T : Actual cell temperature

T_r : Reference cell temperature (298 K)

λ : Actual irradiance

λ_r : Reference irradiance (1000 W/m²)

k_i : Short-circuit current temperature coefficient.

I_{sc} : Short-circuit current at STC (298 K & 1000 W/m²)

q : Electron charge (1.6×10^{-19} C)

K : Boltzmann constant (1.38×10^{-23} J/K)

E_{gp} : Energy bandgap (1.1 eV)

The photo-generated current I_g is a function of temperature and irradiance and is given as

$$I_g = (I_{sc} + k_i(T - T_r))\lambda/\lambda_r \quad (2.2)$$

The reverse saturation current I_s is formulated as

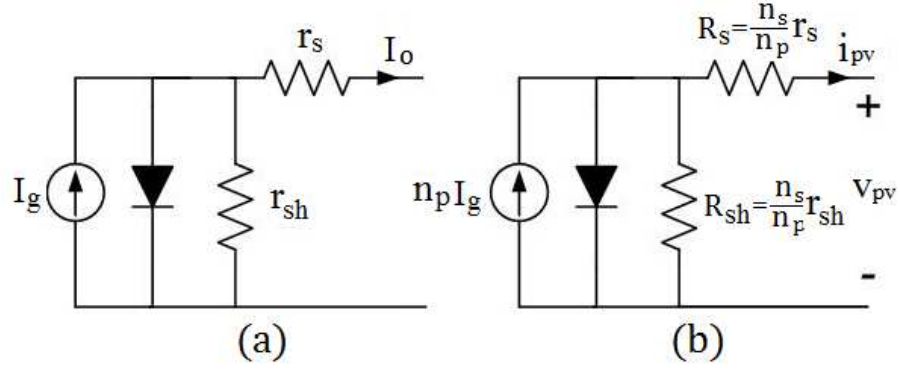


Figure 2.1: Equivalent circuit of (a) Single PV cell (b) Complete PV array

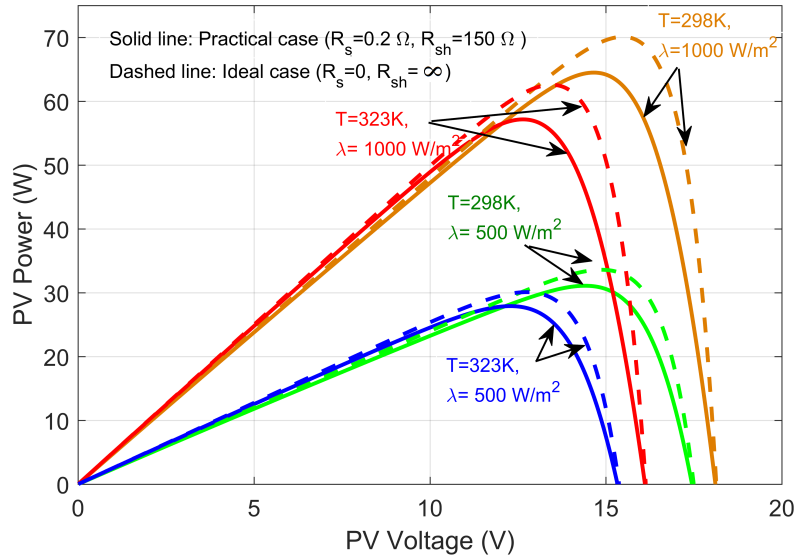


Figure 2.2: Effect of series and shunt resistance of P-V curve for different temperature and irradiance.

$$I_s = I_r \left(\frac{T}{T_r} \right)^3 e^{qE_{gp} \left(\frac{1}{T_r} - \frac{1}{T} \right) / pK} \quad (2.3)$$

As discussed earlier, the variations in irradiance and temperature affect the power output of the solar PV array. Similarly, series and shunt resistances also affect the output power. These effects have been portrayed in the P-V characteristics as shown in Fig.2.2. It may be observed that although R_s and R_{sh} have least effect in open circuit and short circuit region, they greatly influence the P-V characteristic in MPP region. Therefore, it is important to take them into consideration while estimating actual T and λ using I-V curve. Although R_s and R_{sh} vary with T & λ [57], [58], their variation do not cause significant effect on I-V and P-V characteristic as far as T & λ are in operating region. Therefore, we have assumed R_s and R_{sh} to be constant in our method.

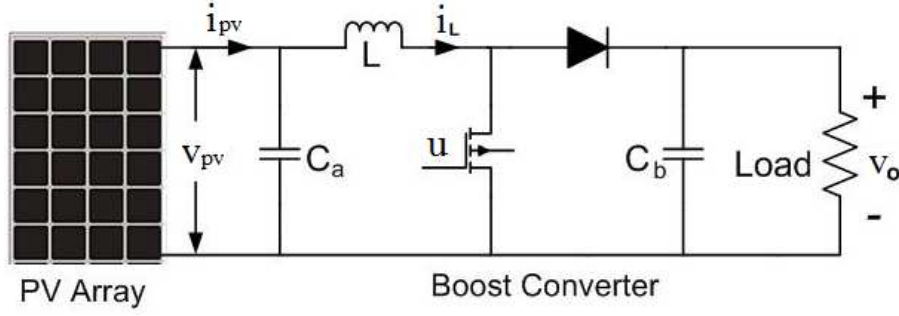


Figure 2.3: PV Array in conjunction with dc-dc boost converter.

2.2.2 Power Converter

Fig. 2.3 shows a PV array connected to a dc-dc boost converter. Power output from PV module is controlled by varying the duty ratio of boost converter so as to operate at MPP. The PV system along with boost converter is a third order non-linear system. Taking inductor current i_L , PV voltage v_{pv} and load voltage v_o as system states, the time averaged state space model of boost converter [59] is described as follows,

$$\dot{i}_L = \frac{1}{L} (v_{pv} - r i_L - V_D - v_o) + \frac{1}{L} (V_D + v_o) u \quad (2.4)$$

$$\dot{v}_{pv} = \frac{1}{C_a} (i_{pv} - i_L) \quad (2.5)$$

$$\dot{v}_o = \frac{1}{C_b} \left(i_L - \frac{v_o}{R_{ld}} \right) - \frac{1}{C_b} i_L u \quad (2.6)$$

Here C_a : PV capacitor, C_b : output capacitor, V_D : diode voltage drop, r : resistance of inductor, R_{ld} : load resistance. u is a switching signal which is 1 when switch is on and 0 when switch is off.

2.3 Temperature and Irradiance Detection

The I-V characteristics of a particular PV array depends on a number of parameters as described in equations (2.1) to (2.3). Temperature and irradiance level can be considered as external parameters which change with environmental condition. Other parameters like ideality factor and modeled resistances of PV array are considered as internal parameters which are known and constant. Therefore, variation in I-V characteristic corresponds to the variation in PV array external parameters. These parameters can be calculated by plugging in different sets of sensed PV array

voltage and current values in system equation. Since the I-V characteristic follows a non linear relation, NR method is used to find the system parameter as it converges faster than other techniques.

The I-V relation can be written as function of internal and external parameters as

$$i_{pv} = f(\mathbf{x}, T, \lambda, v_{pv})$$

where \mathbf{x} is set of internal parameters of PV array which are considered constant.

Following the prescripts of NR Method, it is assumed that (v_1, i_1) and (v_2, i_2) are two sets of measured value of PV array voltage and current at time t and $t + \delta t$ while operating at temperature T and irradiance λ . δt is the time interval at which temperature and irradiance are updated. Hence, i_{pv_1} and i_{pv_2} at v_{pv_1} and v_{pv_2} can be written as

$$i_{pv_1} = f(\mathbf{x}, T, \lambda, v_{pv_1}) \quad i_{pv_2} = f(\mathbf{x}, T, \lambda, v_{pv_2})$$

It is also assumed that $i_{pv_{1k}}$ and $i_{pv_{2k}}$ are the calculated currents at voltages $v_{pv_{1k}}$ and $v_{pv_{2k}}$ respectively in the k^{th} iteration corresponding to estimated temperature T_k and irradiance λ_k . Therefore,

$$i_{pv_{1k}} = f(\mathbf{x}, T_k, \lambda_k, v_{pv_1}) \quad i_{pv_{2k}} = f(\mathbf{x}, T_k, \lambda_k, v_{pv_2})$$

Having known the internal parameters and sets of measured values of PV voltage and current, temperature T_{k+1} and irradiance λ_{k+1} in the next iteration is calculated as follows

$$\begin{bmatrix} T_{k+1} \\ \lambda_{k+1} \end{bmatrix} = \begin{bmatrix} T_k \\ \lambda_k \end{bmatrix} + [J]^{-1} \begin{bmatrix} i_{pv_1} - i_{pv_{1k}} \\ i_{pv_2} - i_{pv_{2k}} \end{bmatrix} \quad (2.7)$$

where

$$[J] = \begin{bmatrix} \frac{\partial i_{pv}}{\partial T} (v_{pv_1}, T_k, \lambda_k) & \frac{\partial i_{pv}}{\partial \lambda} (v_{pv_1}, T_k, \lambda_k) \\ \frac{\partial i_{pv}}{\partial T} (v_{pv_2}, T_k, \lambda_k) & \frac{\partial i_{pv}}{\partial \lambda} (v_{pv_2}, T_k, \lambda_k) \end{bmatrix} \quad (2.8)$$

$\frac{\partial i_{pv}}{\partial T}$ is found out by differentiating (2.1) and then upon simplification is written as

$$\begin{aligned} \frac{\partial i_{pv}}{\partial T} = & n_p \frac{\partial I_g}{\partial T} - n_p \frac{\partial I_s}{\partial T} \left(e^{\frac{q(v_{pv} + i_{pv}R_s)}{pKn_sT}} - 1 \right) - \\ & n_p I_s \frac{\partial}{\partial T} \left(e^{\frac{q(v_{pv} + i_{pv}R_s)}{pKn_sT}} - 1 \right) - \frac{\partial}{\partial T} \frac{(v_{pv} + i_{pv}R_s)}{R_{sh}} \end{aligned} \quad (2.9)$$

Taking the terms of $\frac{\partial i_{pv}}{\partial T}$ together, we get,

$$\frac{\partial i_{pv}}{\partial T} = \frac{n_p k_I \frac{\lambda}{\lambda_r} - n_p \frac{\partial I_s}{\partial T} \left(e^{\frac{q(v_{pv} + i_{pv}R_s)}{pKn_sT}} - 1 \right) + \frac{n_p I_s q(v_{pv} + i_{pv}R_s)}{pKn_s T^2} \left(e^{\frac{q(v_{pv} + i_{pv}R_s)}{pKn_sT}} \right)}{1 + \frac{n_p I_s q R_s}{pKn_s T} \left(e^{\frac{q(v_{pv} + i_{pv}R_s)}{pKn_sT}} \right) + \frac{R_s}{R_{sh}}} \quad (2.10)$$

$$\frac{\partial I_s}{\partial T} = \frac{I_r}{T_r^3} \left(3T^2 + \frac{qE_{gp}T}{pK} \right) e^{\frac{qE_{gp}}{pK} \left(\frac{1}{T} - \frac{1}{T_r} \right)} \quad (2.11)$$

Similarly $\frac{\partial i_{pv}}{\partial \lambda}$ can be written as

$$\frac{\partial i_{pv}}{\partial \lambda} = \frac{n_p (I_{sc} + k_I(T - T_r))}{\lambda_r + \frac{\lambda_r n_p I_s q R_s}{pKT n_s} \left(e^{\frac{q(v_{pv} + i_{pv}R_s)}{pKn_sT}} \right)} \quad (2.12)$$

NR method converges very quickly and it typically takes 4 to 5 iterations to find out the solution of T and λ . The interval δt is also an important parameter which should be carefully chosen. While higher value of δt makes the detection slower in case of change in environmental conditions, smaller value repetitively calculates the same T and λ with high frequency in case of no environmental change. To overcome this situation, in this work, the new value of T and λ is estimated only when change in PV voltage/current is greater than a minimum value.

2.4 Calculation of desired states

Desired states of the system are calculated using state space equations once the PV characteristic is known. PV voltage v_{pv_r} and current i_{pv_r} corresponding to MPP are

Table 2.1: Desired values of PV voltage, Current and Power for different environmental conditions

Case	Temperature	Irradiance	v_{pv_r}	i_{pv_r}	P_{pv_r}
I	298K	$500W/m^2$	14.4V	2.15A	31.0W
II	298K	$1000W/m^2$	14.6V	4.40A	64.2W
III	323K	$1000W/m^2$	12.7V	4.52A	57.5W
IV	323K	$500W/m^2$	12.3V	2.26A	28.5W

numerically found out using INC method as done in [60]. Calculation of desired value of inductor current and converter output voltage is performed using steady state analysis.

Let i_{L_r} , v_{pv_r} , v_{o_r} be the desired steady-state values of inductor current, PV voltage and converter output voltage respectively and $e_1 = i_L - i_{L_r}$, $e_2 = v_{pv} - v_{pv_r}$, $e_3 = v_o - v_{o_r}$ be their corresponding errors. In steady state, when the desired values are reached, all the errors and their derivatives become 0.

$$e_1 = e_2 = e_3 = 0, \dot{e}_1 = \dot{e}_2 = \dot{e}_3 = 0 \quad (2.13)$$

Therefore, in steady state, (2.4) to (2.6) become

$$\frac{1}{L}(v_{pv_r} - ri_{L_r} - V_D + u_r V_D - v_{o_r} + u_r v_{o_r}) = 0 \quad (2.14)$$

$$\frac{1}{C_a}(i_{pv_r} - i_{L_r}) = 0 \quad (2.15)$$

$$\frac{1}{C_b} \left(i_{L_r}(1 - u_r) - \frac{v_{o_r}}{R_{ld}} \right) = 0 \quad (2.16)$$

Upon simplifying, (2.14), (2.15) and (2.16) we get,

$$i_{L_r} = i_{pv_r} \quad (2.17)$$

$$v_{o_r} = \frac{-V_D + \sqrt{V_D^2 + 4i_{pv_r}R_{ld}(v_{pv_r} - ri_{pv_r})}}{2} \quad (2.18)$$

$$u_r = 1 - \frac{v_{pv_r} - i_{pv_r}r}{V_D + v_{o_r}} \quad (2.19)$$

where u_r is the desired duty cycle.

Equations (2.17) to (2.19) show that the desired steady state inductor current is equal to the reference PV current corresponding to MPP. Although desired PV current for MPP and hence desired average inductor is independent of load, the final output voltage is a function of load resistance which makes the desired duty cycle dependent on load. Table 2.1 shows desired values of MPP PV voltage, current and power for different temperature and irradiance levels. These desired states can be achieved by a range of controllers which include different varieties of linear and non-linear techniques.

2.5 Simulation Results and Discussion

The performance of the proposed algorithm is simulated using MATLAB 2016a software on Intel core i3, 2.4GHz processor, 4GB RAM and Windows 7 operating system. PV array block has been used to simulate solar array. The operating temperature and irradiance can be given as external input and varied as desired. The parameters of the PV array block is shown in Table 2.2. The pattern of variation in temperature and irradiance is shown in Fig. 2.4. The reference PV voltage and current values are given in Table 2.1 for these four cases. The estimated value of temperature and irradiance are obtained in Fig. 2.5 and Fig. 2.6 respectively using the procedure discussed in Section 2.4. It can be observed that the variation of estimated values are within 0.5% of their actual values. These values are estimated at the interval of 0.05s. It is also observed that the two parameters reach their steady state value within 0.25s. Although temperature is changed at $t = 2s$, there are some transients in estimated temperature at $t = 1s$ and $t = 3s$. Similarly transients are observed in irradiance estimation at $t = 2s$ when it is changed at $t = 1s$ and $t = 3s$. These transients are due to the fact that the calculation of one parameter is not independent from another. The P-V curve is changed if any of these two parameters is changed. These parameters cannot be correctly calculated if the two sets of voltage and currents are from different P-V curves. Once the P-V characteristic settles on a single curve, the parameter estimation is correctly done.

Figures 2.7 and 2.8 show the dynamics of desired, estimated and actual values of PV voltage and PV power respectively. Temperature and irradiance of PV array block are changed as per Fig. 2.4. Time taken to reach steady state values is 0.05s. The desired, calculated and actual inductor current is shown in Fig. 2.9. It is to be noted that calculated inductor current tracks the actual current. The steady state ripple in calculated inductor current is much lower compared to its actual value because the calculated inductor current is function of PV voltage and PV current which are constant in steady state. However, these transients are present in calculated inductor current whenever there is variation in operating conditions. The

Table 2.2: parameters used for simulation and hardware implementation

PV array parameter		Circuit parameter	
T_r	298K	C_a	$200\mu F$
λ_r	$1000W/m^2$	C_b	$200\mu F$
p	1	L	5mH
I_r	$1.37 \times 10^{-8}A$	r	0.2Ω
I_{sc}	4.8A	V_d	0.6V
R_s	0.2Ω	Controller parameter	
R_{sh}	150 Ω	f_s	20KHz
n_s	36	K_c	1.5
n_p	1	t_o	0.025s
		∂t	0.05s

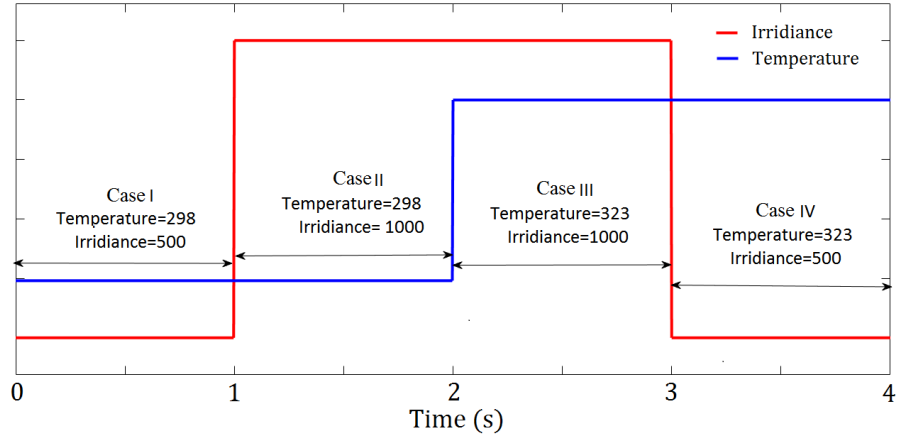


Figure 2.4: Different cases of variation in temperature and irradiance

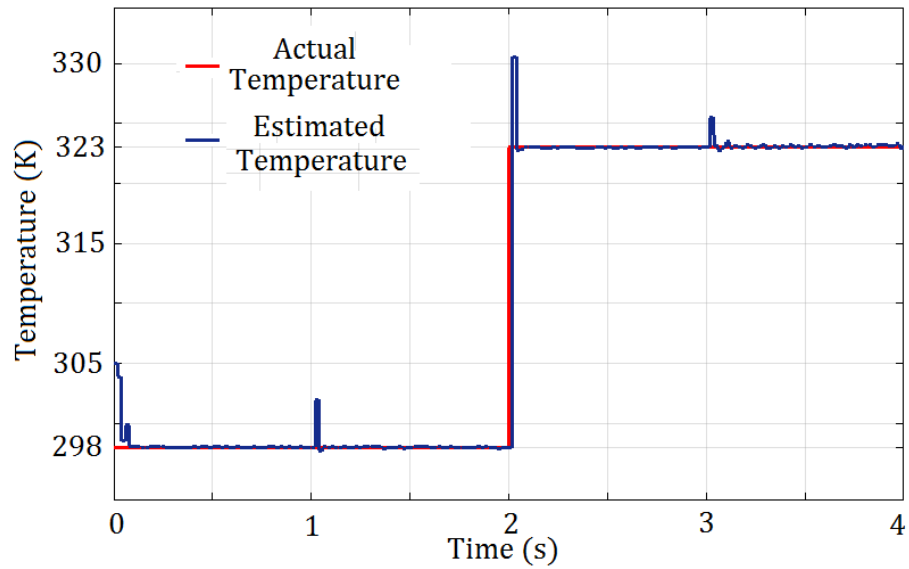


Figure 2.5: Comparison of estimated temperature with actual value

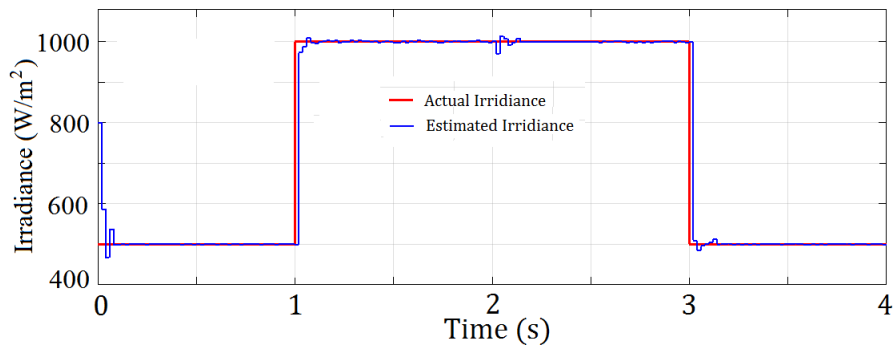


Figure 2.6: Comparison of estimated irradiance with actual value

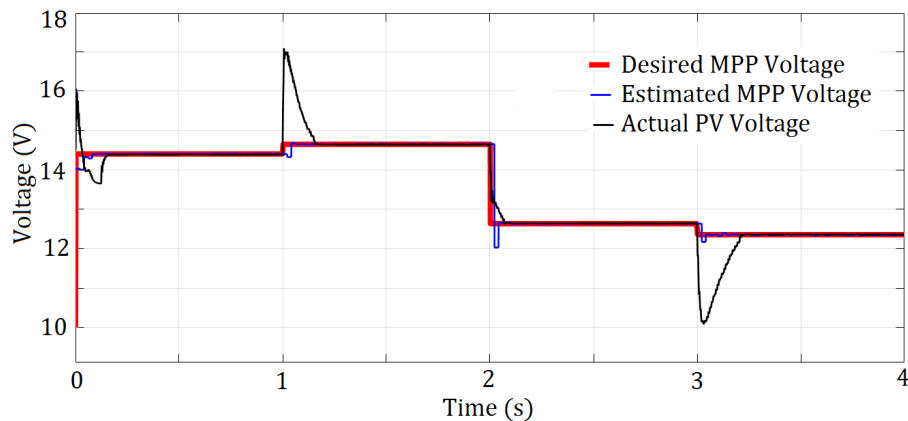


Figure 2.7: Desired voltage, estimated voltage and actual current for MPP under different environmental conditions.

transient time depends on the input capacitor value. Fig.2.10 shows the variation in PV voltage, power and duty ratio when load is changed.

2.6 Summary

This chapter presents a fast MPPT technique for photovoltaic array by estimating environmental conditions and load. For temperature and irradiance estimation, Newton-Raphson method has been applied to I-V characteristic of the PV array. Load was estimated by calculating inductor current and load voltage using boost converter dynamics. Simulation results show that the proposed method is able to operate the PV array at MPP under varying environmental and load conditions. The proposed method is able to find the value of duty cycle in single step for MPPT which otherwise is gradually found. This enables the proposed method to be free from multiple transients during MPPT and steady state oscillation. Application of proposed method to the case of partial shading will be carried out in the future.

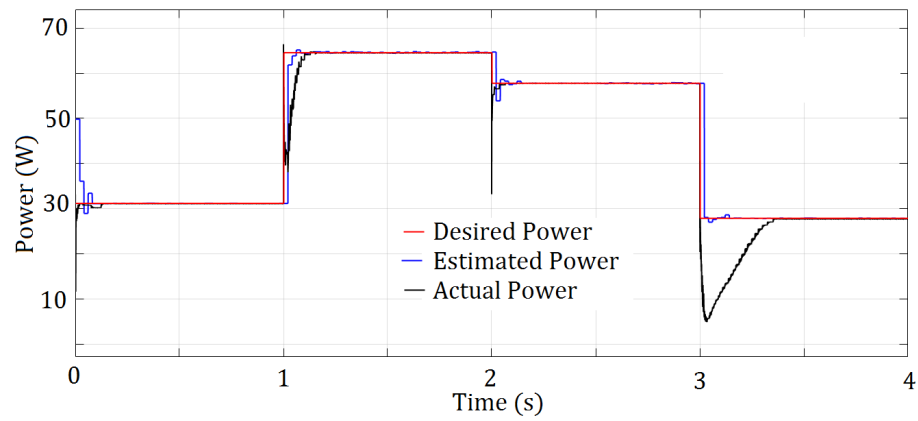


Figure 2.8: Desired Power, estimated power and actual power for MPP under different environmental conditions.

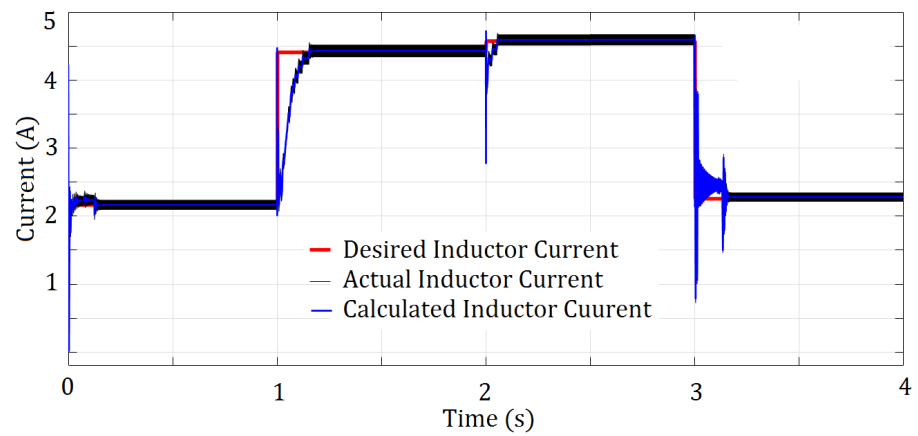


Figure 2.9: Desired, calculated and actual inductor current at MPP for different environmental conditions

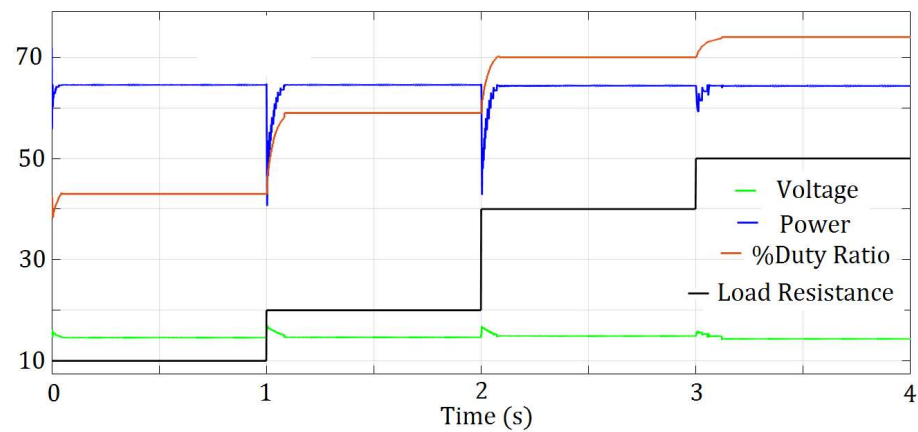


Figure 2.10: PV voltage, power and duty ratio for different load conditions

Chapter 3

A Unified Sensor-free Control Strategy for MPPT and Voltage Control in Standalone PVDG Systems

In this chapter, a description is given on developing a unified control approach for mppt and voltage control without placing any sensors near the PV array. This has been achieved keeping in mind the power balance conditions of the Standalone PVDG system.

3.1 Introduction

In SPVDGs, DC bus voltage control and MPPT are generally carried out separately. An extensive treatment of various MPPT techniques has already been done in the previous chapter and the voltage control carried out by many linear and nonlinear approaches with different higher level control structures like autonomous control, coordination control and supervisory control [61]. All of these methods require different sets of voltage and current sensors for both the control tasks of the SPVDG namely MPPT and DC voltage control.

Inorder to scale these technologies to the underprivileged parts of the world where SPVDGs are actually required, any technique which would reduce the cost of the system is very much welcome. By developing intelligent methods to reduce sensors, it is possible to reduce the overall cost of the system. The concept of sensor reduction in SPVDG systems is hardly explored in literature although it had been very much considered in drive based systems. For instance, [62] uses observers to remove the current sensor on the PV array side necessary for tracking MPPT. [63]

proposes using only averaged voltages of a photovoltaic array and the average duty ratios to eliminate the current sensor in the MPPT process. [64] discusses how to use only one sensor in ESS control for DC voltage stabilization in SPVDG system. However, none of them provide any solution to carry out both MPPT and voltage control with reduced sensors.

With these concerns, this chapter proposes a direct perturbation based MPPT algorithm for a standalone DC microgrid which requires no sensor to be placed with the PV array side. A set of logic conditions are derived with respect to any change in grid voltage. The conditions are processed within an algorithm to decide the next perturbation for reaching MPP. More importantly, this single algorithm not only serves for MPPT but also accomplishes DC bus voltage control which is an ancillary service in a conjoint manner. Automatic battery charging and discharging is carried out through seamless transition between buck and boost modes of operation based on grid voltage operating condition. This is facilitated by a bidirectional converter (BDC) used for integrating BESS to the DC grid which enables two way power flow from battery to grid and vice-versa. It uses the duty ratios for BDC by generating them previously MPP section.

In essence, a unique and indirect method to achieve MPPT and DC grid voltage control without any sensors connected to PV array for MPPT has been presented in this chapter. An integrated algorithm is developed which exploits the natural electrical interconnection between both the PV and battery subsystems to achieve both MPPT and ancillary service like voltage control in a concomitant manner. This method is very simple with negligible computational burden and carries out two functions in a single control module. It is a low cost method as it uses less sensors.

The following is the organization of this chapter. Section 3.2 describes the SPVDG system under consideration and its working. Section 3.3 gives a comprehensive understanding of the direct perturbation based unified MPPT and voltage control technique. Section 3.4 shows the results that are obtained for the MATLAB/Simulink simulations while Section 3.5 concludes the chapter.

3.2 Configuration Of the SPVDG

A solar photovoltaic based low voltage SPVDG unit is proposed for this work. It operates off-grid with local generation from solar PV and feeds local DC loads. It basically contains both DC/DC boost and BDC with a battery storage device and resistive load. A complete circuit model of the proposed system is given in Fig.3.1.

The PV source is simulated by taking SLX060 USC solar module from simulink library. It generates photovoltaic current (i_{pv}) and voltage (V_{pv}) to meet up with the

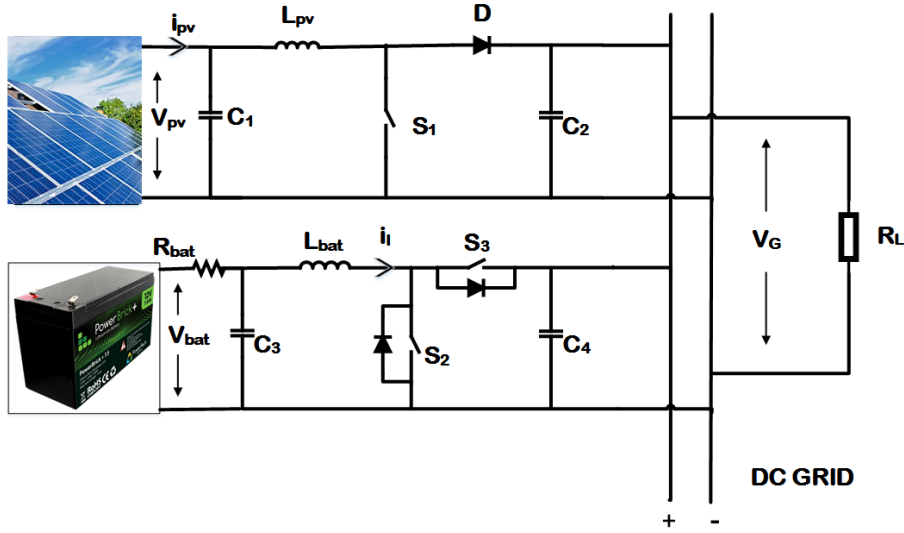


Figure 3.1: Overall schematic of the standalone DC microgrid.

maximum power rating. A PV cell is the very basic element of an array comprises of a p-n junction diode which converts the solar irradiation into electric energy. The solar module contains 36 number of series connected cells to generate required amount of PV output voltage.

The equivalent circuit of PV cell and an array can be seen in Fig. 3.2 where n_s and n_p are number of cells in series and parallel respectively.

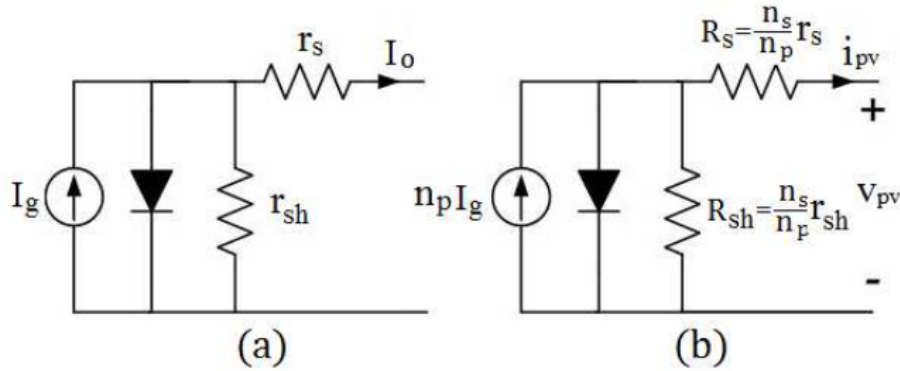


Figure 3.2: Equivalent circuit of (a) single PV cell (b) PV array.

A DC/DC boost converter boosts up the PV voltage to a suitable DC reference value at the DC bus through a MPPT algorithm. It is properly modeled with accurate parameters for a unidirectional power flow from PV source to grid [65]. The switching signal for proper duty cycle is computed by proposed direct perturbation based MPPT algorithm. The output pulse is given to gate of the switch to produce required V_G to be appeared at DC load bus.

A DC/DC bi-directional converter is used to integrate a BESS battery to the

DC grid. It enables bi-directional power flow from grid to battery and vice-versa to establish automatic battery charging and discharging by eventually controlling the DC grid voltage [66]. Dynamic values of duty cycles for both buck and boost operation are calculated by the proposed control algorithm and fed to the respective gate port of the switches. Both the converters use MOSFET switches(S_1, S_2, S_3) for their characteristics of being used in low voltage applications (10-100 volts, 10-100 KHz switching frequency).

The BESS consists of a Li-ion battery and is based on the dynamic run time characteristics such as non-linear open circuit voltage, current dependency of storage duration and effective response to transients. A dynamic resistive load is connected at output considered as the point of DC grid because of the absence of synchronization and frequency related issues in case of the DC system on study. Parameters for all the sub systems and elements are given in Table 3.1.

Table 3.1: Parameter Specification

Subsystem	Parameter Specification
PV Array at STC	Model: SLX 230 USC module $V_{OC} = 16V, I_{SC} = 4.8A$ $V_{MPP} = 14.6V, I_{MPP} = 4.4A$
Battery	Model: Lithium Ion: 15V
DC/DC Converter	$C_1 = 100\mu F, C_2 = 500\mu F, L_{pv} = 0.35mH$ $f_{sw} = 10kHz$ for S_1
DC/DC Bidirectional Converter	$C_3 = 100\mu F, R_{bat} = 0.3\Omega, L_{bat} = 0.3mH$ $f_{sw} = 10kHz$ for S_2 and S_3
PI Gains	$K_{pv} = 0.2, K_{iv} = 0.1$ $K_{pi} = 0.2, K_{ii} = 0.01$

3.3 Unified Sensorless Control Strategy

The proposed control strategy focuses on developing an efficient algorithm which governs both of the following tasks:

1. Direct perturbation based sensor-free MPP tracking and
2. Automatic battery charging/discharging with seamless mode transition for DC grid voltage control.

The algorithm works in such a novel way that in a single work space not only it tracks MPP but also carries out efficient charging and discharging of a battery

by instant transition from buck to boost mode and vice-versa with respect to grid voltage operating conditions for the proposed standalone DC microgrid. A nested control structure is proposed which relates all the control inputs and outputs to operate in an integrated form and is well understood from block diagrams in Fig. 3.3. Duty ratios calculated in one section of the algorithm are simultaneously used by voltage and current loops to decide the mode of operation for bi-directional converter.

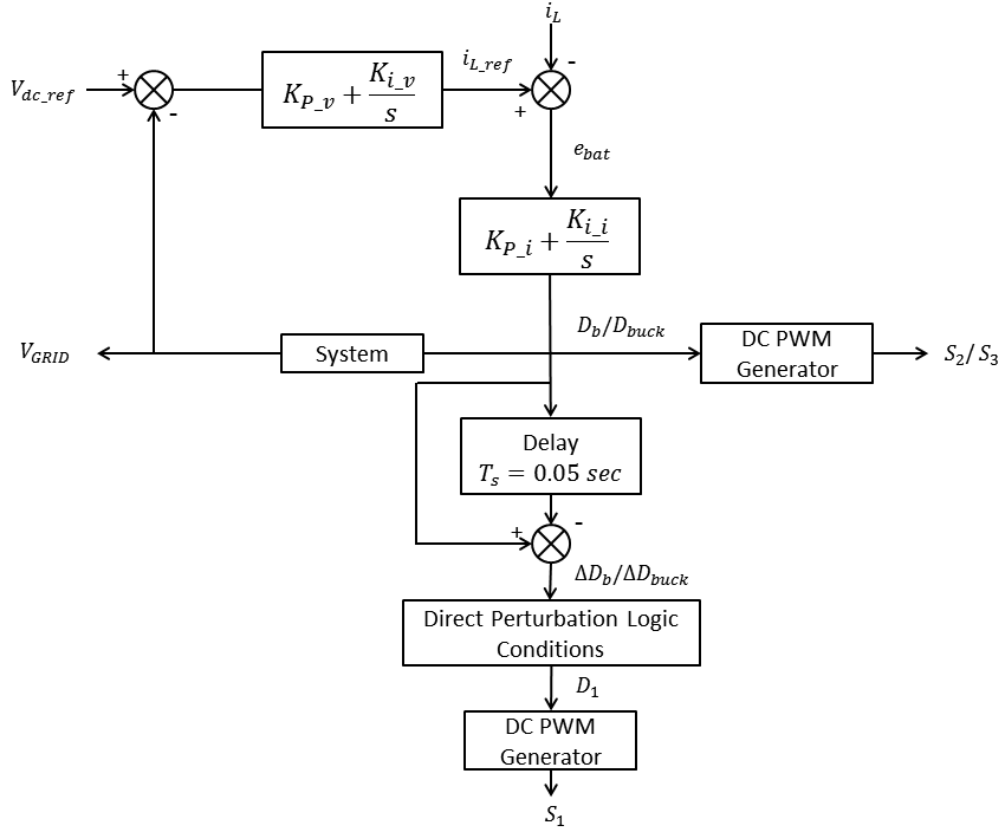


Figure 3.3: Control strategy for MPPT and DC bus voltage control

3.3.1 Direct perturbation based sensor-free MPP tracking

In this approach, a new direct perturbation based sensor-free MPPT algorithm is developed. Unlike the basic P&O method, the current algorithm does not use any sensor measurement at PV array to observe a corresponding change in power; instead the change in power is estimated by observing the grid voltage sensor measurement. On which the decision is appropriately taken automatically which gradually progresses towards MPP; hence the name direct perturbation based is given. If a perturbation on duty cycle of the boost converter causes an increase in PV power, it will momentarily increase the grid voltage. This change is sensed by a voltage sensor and provides it to the PI controller. The output of PI controller is the duty

cycle of buck mode of operation for bi-directional converter which will be decreased in steps to reduce the supplied power from battery so that excess power caused by perturbation can be counter balanced. Therefore a reduction in that duty cycle can be viewed as increase in PV power and hence decision of perturbation can be continued in same direction (considered as positive). Similarly decision to reverse the direction of perturbation (negative) is taken if the corresponding duty cycle increases as an effect to restore the grid voltage.

The whole instructions work in a cause-effect relationship. A change in duty ratio of the boost converter ΔD_{pv} associated directly with the PV source is considered as the cause. Change in duty ratio of either buck or boost mode of bi-directional converter ($\Delta D'_b$ or ΔD_b) is the effect. In every iteration, the sign of the quantities $\Delta D_{pv} \times \Delta D_b$ and $\Delta D_{pv} \times \Delta D'_b$ are checked to take decision on next perturbation. The algorithm approaches MPP by continuously executing the set of conditions given in Table 3.2 and Table 3.3. A small part of the algorithm is illustrated as follows:

$$\begin{aligned}
\Delta D_{pv} &= D_{pv} - D_{pv_{old}}; \\
\Delta D_b &= D_b - D_{b_{old}} \\
if(mod(t, 0.05) == 0) \\
if(\Delta D_{pv} * (\Delta D_b) > 0; \\
D_{pv_n} &= D_{pv} - delD; \\
D_{pv_{old}} &= D_{pv}; \\
D_{pv} &= D_{pv_n}; \\
D_{b_{old}} &= D_b;
\end{aligned} \tag{3.1}$$

Where D_{pv} and D_b are the duty ratio of boost converter and boost mode operation of BDC. The same way computation is done for other set of conditions given in Table 3.2 and Table 3.3.

Table 3.2: Set of conditions for buck operation

S.No	Cause ΔD_{pv}	Effect $\Delta D'_b$	Product $\Delta D_{pv} * \Delta D'_b$	Decision ΔD_{pv}
Case-1	Positive	Positive	Positive	Positive
Case-2	Positive	Negative	Negative	Negative
Case-3	Negative	Positive	Negative	Negative
Case-4	Negative	Negative	Positive	Positive

Table 3.3: Set of conditions for boost operation

S.No	Cause ΔD_{pv}	Effect ΔD_b	Product $\Delta D_{pv} * \Delta D_b$	Decison Decision ΔD_{pv}
Case-1	Positive	Positive	Positive	Negative
Case-2	Positive	Negative	Negative	Positive
Case-3	Negative	Positive	Negative	Positive
Case-4	Negative	Negative	Positive	Negative

3.3.2 Automatic battery charging/discharging with seamless mode transition for DC grid voltage control

The objective of this section is to control the automatic charging and discharging of the battery system while performing the MPPT. For this a dual loop PI controller is applied constituting an inner current and outer voltage loop. The current loop works with more speed than the voltage loop due to the faster dynamics associated with current. The inner loop checks the direction of inductor current associated with BESS while the outer loop takes care about the DC grid output voltage. Firstly the difference of reference DC ($V_{dc_{ref}}$) and grid voltage (V_G) is processed through a simple PI controller to get the reference value for battery inductor current ($i_{l_{ref}}$). Another PI controller associated with the inner loop gives rise to D_b and D'_b from the difference between ($i_{l_{ref}}$) and (i_l). This can be expressed as below:

$$i_{l_{ref}} = (V_{dc_{ref}}(s) - V_G(s)) \times (K_{pv} + \frac{K_{iv}}{s}) \quad (3.2)$$

$$D_b = (i_{l_{ref}}(s) - i_l(s)) \times (K_{pi} + \frac{K_{ii}}{s}) \quad (3.3)$$

$$D'_b = -(i_{l_{ref}}(s) - i_l(s)) \times (K_{pi} + \frac{K_{ii}}{s}) \quad (3.4)$$

where K_{pv}, K_{iv} and K_{pi}, K_{ii} are proportional and integral controller gains for voltage and current loops respectively, D_b and D'_b are duty ratios of boost and buck mode of operation respectively for the BDC. Depending on the output of PI controller, the BDC operates in two modes as follows:

- When $i_{l_{ref}} < 0$, BDC operates in buck mode and excess power is given back to the storage device to restore DC bus voltage and it gets charged. The algorithm with set of logic conditions for buck operation is tabulated in Table 3.2.

- When $i_{l_{ref}} > 0$, BDC operates in boost mode and shortage of power is supplied by the storage device to the DC bus and again controlling its voltage to a reference value. The algorithm for boost operation is tabulate in Table 3.3.

The transition from buck to boost mode and vice-versa is done smoothly without any considerable delay so that the system outage is avoided. The whole process can be summed up by following equations:

$$\begin{aligned}
 & if(mod(t, 0.0002) == 0) \\
 & \quad e_{bat} = i_{l_{ref}} - i_l \\
 & \quad sum = sum + e_{bat} \\
 & \quad if(i_{l_{ref}} > 0) \\
 & \quad \quad D_b = K_{p_i} * e_{bat} + K_{i_i} * sum; \\
 & \quad if(i_{l_{ref}} < 0) \\
 & \quad \quad D'_b = -(K_{p_i} * e_{bat} + K_{i_i} * sum);
 \end{aligned} \tag{3.5}$$

3.4 Simulation Results

The complete low voltage DC microgrid circuit is designed and implemented using MATLAB Simulink. The circuit parameter for the simulation is taken from Table 3.1. The grid reference voltage is set at 20 V and load resistance is taken to be 10Ω. Initially solar irradiance is set at 1000 W/m². Its value is decreased to 800 W/m² at 0.25 s of the simulation. The irradiance is further decreased to 500 W/m² at 0.5 s and then increased to 750 W/m² at 0.75 s. The variation of solar power due to change in solar irradiance is shown in Fig. 3.4.

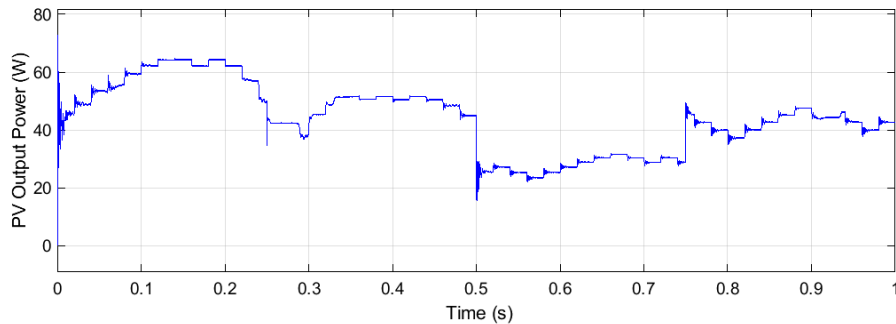


Figure 3.4: PV power variation due to change in solar irradiance

From 0 s. to 0.25 s and from 0.25 s to 0.5 s, BDC works in buck mode indicating that excess of power at DC bus being supplied to the battery to restore 20 Volts at DC bus. In this mode of operation, current direction is negative so that battery

gets charged. This is clearly depicted in Fig. 3.5 where reference inductor current is below zero up to 0.05 s justifying the accurate control action.

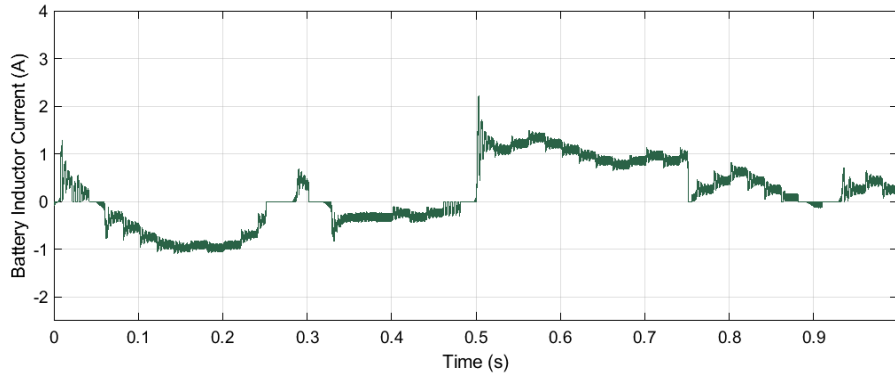


Figure 3.5: Inductor current associated with BESS

Due to irradiance reduction after 0.5s, the voltage at load side tends to change. But the control strategy has to restore the dc bus or load voltage. Therefore BDC has to operate in boost mode so that shortage of PV power at load side is required to supply from battery. In this action the battery discharges and its current starts to flow towards load indicating its reference value above zero.

The corresponding duty ratios for buck and boost mode of operation respectively is given by D'_b and D_b can be seen in Fig. 3.6. It shows the corresponding buck and boost transition is smoothly done with respect to grid voltage operating condition. It is carried out without any delay to avoid unnecessary outages in the system.

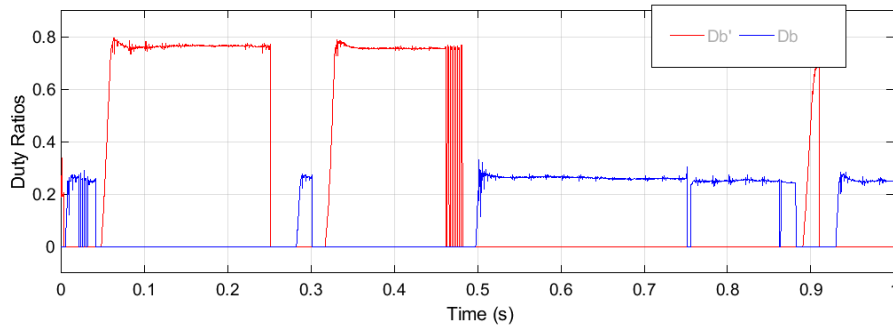


Figure 3.6: Duty ratio of buck and boost operation

Fig. 3.7 shows that the output voltage at DC bus/grid remains constant at a set reference value so that during any disturbance controller restore the voltage and constant power is supplied to the load.

The results show that the developed closed loop system is extremely stable when disturbances occur in the form of irradiance change. A detailed stability analysis of the closed loop system was carried out after omitting the high speed inner current loop. However, due to lack of space, this has been omitted.

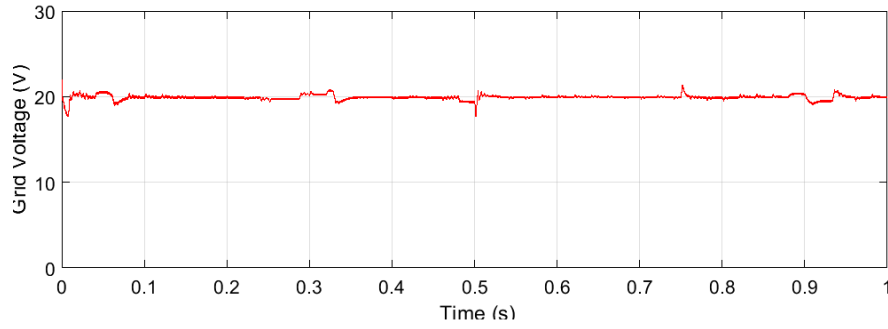


Figure 3.7: DC bus voltage

3.5 Summary

A direct perturbation based sensor-free MPPT with DC bus voltage control is presented for a standalone DC microgrid unit. In this method MPPT is achieved without using any sensor on PV array side. The controller is able to track the MPPT according to change in the duty ratio of BDC with reference to grid voltage condition. The dual loop PI controller controls the power flow in both the ways by checking the direction of reference inductor current, thus carries out effective battery charging/discharging. The transition from buck to boost mode is done efficiently without any delay. From simulation results it is clear that the control algorithm not only regulates DC bus/ grid voltage but also operates PV array at MPP at low cost.

Chapter 4

A Nonlinear Back-stepping based Controller for Standalone PVDG Systems

In this chapter, we will focus on developing a control technique for SPVDG system to tackle various large disturbances with the help of back-stepping strategy. It is interesting to see how a seemingly generalized nonlinear system model has been viewed in a piece-wise strict-feedback format so that back-stepping could be applied satisfactorily. Towards the end, the application of this control technique to various large disturbance is studied and evaluated.

4.1 Introduction

Managing the power flow with advanced control strategies has become unavoidable in SPVDG systems and are generally sorted out by adopting a hierarchical control structure. The major control challenges for an SPVDG with battery energy storage are maximum power point tracking and DC voltage control.

The authors in [67], [68] propose a model predictive control technique on a boost converter setup. However, the controller design is linear in nature which makes enables the system to operate only in a limited manner. It is limited in the sense that it does not cater to large changes in operating points. [69] describes a passivity type controller for a similar boost converter setup but the system is very sensitive to exact parameter tuning which may create problems during implementation. [70] adopts a sliding mode based design to appropriately charge or discharge the battery to maintain voltage. However, lot of precaution needs to be taken to select a sliding surface that can avoid unnecessary switching during sudden disturbances.

In course of its operation, an SPVDG encounters a large region of operation

and thus a far advanced and complex control strategy is justified. Backstepping controller is a good choice of controller design as it operates in a larger range of operation especially when the system is underactuated like in the SPVDG case. Moreover, a detailed stability analysis can be carried out with this kind of controllers which is very much desirable for these type of systems. A backstepping type control has been designed in a shipboard power system to control voltage in [71]. [72, 73] applied similar back-stepping technique in microgrids for voltage control.

However, all these works have been developed to target only a specific type of control in their overall system. This chapter develops a generic modular backstepping based design that can be applied for achieving multiple control goals in the SPVDG system. Also, a plug and play approach as the one developed in this work, allows independent operation of each device in system assuring greater flexibility while improving reliability. Finally, the use of such nonlinear techniques also improves the speed of response in case of transients. It is also very easy to scale up to higher order systems with many sub-systems. The systems stability is shown by constructing a series of Lyapunov functions. The overall system then guarantees good dynamic performance along with flexibility.

The following is the organization of this chapter. Section 4.2 describes the SPVDG system under consideration, its mathematical modeling and its control hierarchy. Section 4.4 gives the complete stability proof of the piece-wise back-stepping control along with the designed controllers and observers. Section 4.5 shows the results that are obtained due to occurrence of different intermittencies while Section 4.6 concludes the chapter.

4.2 System Description and Modeling

This section explains the details of different building blocks of the SPVDG system, its control structure and the large signal modeling of the overall system.

4.2.1 Basic Blocks

The SPVDG system under consideration consists of a PV array and a battery energy storage system (BESS) feeding to a load. The PV array continuously extracts power from the available solar energy and transfers it to the load using a DC-DC converter as shown in Fig. 4.2. The BESS is connected to the grid via a bidirectional DC-DC converter. This is essential to modulate power flow in both the directions as demanded by load conditions in the SPVDG system. Both the converters are controlled using to regulate the desired flow of power in the PVDG system.

4.2.2 Hierarchical Control Structure

As evident from Fig.4.1, the hierarchy of control in the SPVDG system is present in two levels of the SPVDG system namely, primary and secondary. The secondary level controller handles the overall energy management function of the SPVDG. It is responsible for ensuring maximum power extraction from the PV panel and also plan the power flow of the battery depending on the imbalance between the PV power generation and load consumption. The secondary controller achieves this operation by setting the reference values for all the important states in the SPVDG system like inductor currents and capacitor voltages. The major function of the primary controller is to bring the system states to the reference values set by the secondary controller. A properly designed primary controller performs this function even in the presence of large disturbances affecting the system time to time.

4.2.3 State Space Model

The power circuit architecture of SPVDG system is shown in Fig.4.2 which is mathematically modelled in this section. The well established State Space Averaging [74] technique is used for modelling the overall system due to abundance of power electronics in the system.

The PV system consists of a PV array whose output current equation is given by (4.1)

$$i_{pv} = n_p I_g - n_p I_s \left(e^{\frac{q(v_{pv} + i_{pv} R_s)}{n_s p K T}} - 1 \right) - \frac{v_{pv} + i_{pv} R_s}{R_{sh}} \quad (4.1)$$

The PV output current i_{pv} varies with change in temperature and irradiance

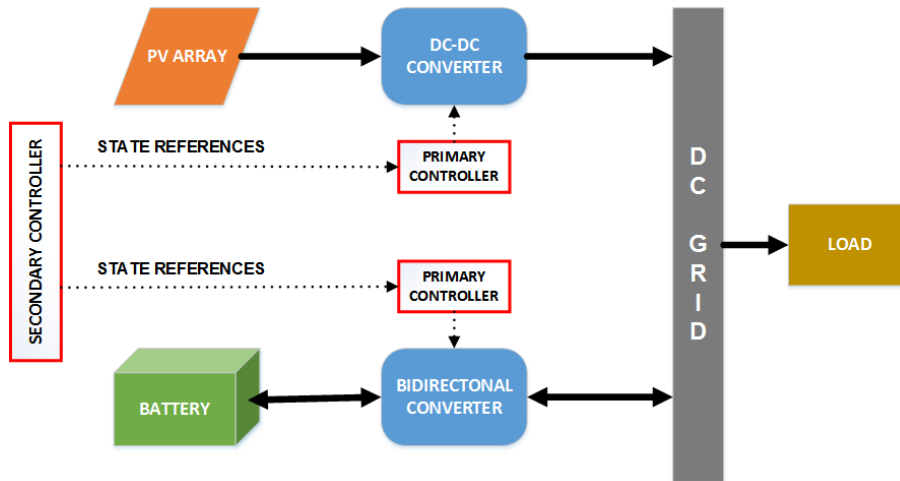


Figure 4.1: Structure of SPVDG System

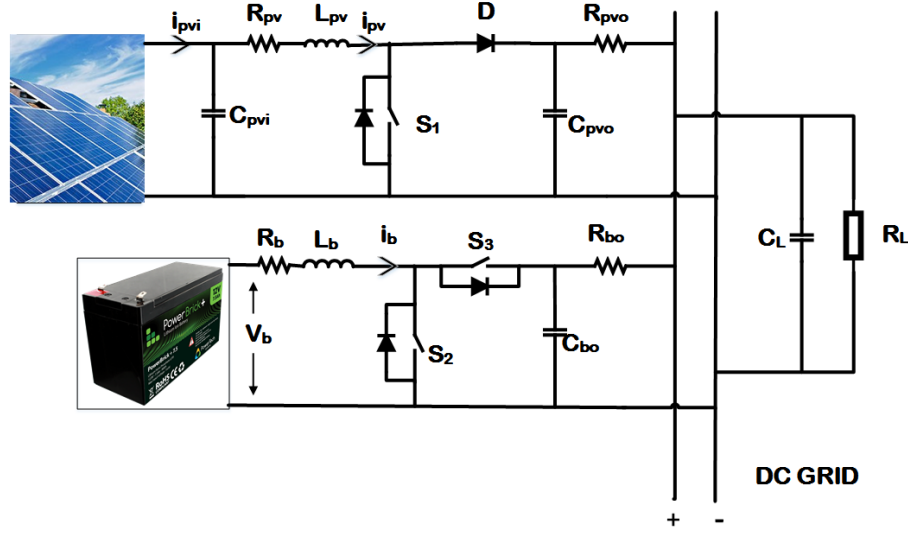


Figure 4.2: Power Architecture of the SPVDG System

and it needs to be continuously monitored. In the state-space model, this current has been considered as disturbance d_1 . The output voltage of PV panel which is also the voltage across capacitor C_{pvi} has been designated as x_1 , the voltage across capacitor C_{pvo} has been termed as x_2 and the current through inductor L_{pv} has been designated x_3 . All these states belong to the PV subsystem.

The battery has been modelled as a voltage source whose voltage is considered as disturbance d_2 . Similarly, the current through inductor L_b has been termed as x_4 and voltage across capacitor C_{bo} has been designated as x_5 . Both these states belong to the battery subsystem. Finally, the DC grid voltage which is the voltage across C_L and is taken to be x_6 and load admittance $\frac{1}{R_L}$ is modeled as disturbance d_3 .

The state space model derived for this system is obtained as follows:

$$\begin{aligned}
\dot{x}_1 &= \frac{d_1}{C_{pvi}} - \frac{x_3}{C_{pvi}} \\
\dot{x}_2 &= \frac{x_3}{C_{pvo}} - \frac{x_2}{R_{pvo}C_{pvo}} + \frac{x_6}{R_{pvo}C_{pvo}} - \frac{x_3}{C_{pvo}}u_1 \\
\dot{x}_3 &= \frac{x_1}{L_{pv}} - \frac{x_2}{L_{pv}} - \frac{x_3R_{pv}}{L_{pv}} + \frac{x_2}{L_{pv}}u_1 \\
\dot{x}_4 &= \frac{d_2}{L_b} - \frac{x_4R_b}{L_b} - \frac{x_5}{L_b} + \frac{x_5}{L_b}u_2 \\
\dot{x}_5 &= \frac{x_4}{C_{bo}} - \frac{x_5}{R_{bo}C_{bo}} + \frac{x_6}{R_{bo}C_{bo}} - \frac{x_4}{C_{bo}}u_2 \\
\dot{x}_6 &= \frac{x_2}{C_LR_{pvo}} + \frac{x_5}{C_LR_{bo}} - \frac{x_6}{C_L} \left[\frac{1}{R_{pvo}} + \frac{1}{R_{bo}} + d_3 \right]
\end{aligned} \tag{4.2}$$

where

$$\begin{aligned}
x &= [V_{pvi} \ V_{pvo} \ i_{pv} \ i_b \ V_{bo} \ V_L] \\
d_1 &= i_{pvi} \quad d_2 = V_b \quad d_3 = \frac{1}{R_L}
\end{aligned}$$

4.3 Reference Generation:

This section shows a technique using which the secondary level references can be generated. The secondary level references are generated by the secondary controller and sent to the primary level controllers so that appropriate control action is taken to follow these secondary level references. Successful calculation/estimation of these references holds the key to power balance of the entire SPVDG system. It also decides whether the bidirectional converter should work in the charging mode or discharging mode.

Since, the state space model of the system is known, by equating the state space equations to zero and solving the equations by eliminating the control variables is the way forward for generating these references. However, it is to be understood that this would not bring the system to work at our desired voltage and current levels. Hence, we need to substitute certain desired voltage and current values in the previous set of equations obtained through equating the state space equations to zero. Then, we will be able to arrive at the set of desired values for all the states in the system.

Let us say that the microgrid needs to operate at a voltage V_{DC} and that the PV output voltage should be maintained at V_{mpp} to ensure maximum power extraction from the panel/array. These two references serve the basis for generating the references of all the states in the system. The following set of equations denote the

values of references used for the current SPVDG system:

$$\begin{aligned}
x_{6ref} &= V_{DC}(known) \\
x_{1ref} &= V_{mpp}(known) \\
x_{3ref} &= I_{mpp}(known) \\
a_1 &= 1 \quad b_1 = -x_{6ref} \\
c_1 &= x_{3ref}^2 R_{pvo} R_{pv} - x_{1ref} x_{3ref} R_{pvo} \\
x_{2ref} &= -b_1 + \sqrt{\frac{b_1^2 - 4a_1 c_1}{2a_1}} \\
x_{5ref} &= -\frac{R_{bo}}{R_{pvo}} x_{2ref} + x_{6ref} \left(1 + \frac{R_{bo}}{R_{pvo}} + \frac{R_{bo}}{R_l} \right) \\
a_2 &= R_{bo} \quad b_2 = -R_{bo} d_2 \\
c_2 &= x_{5ref}^2 - x_{5ref} x_{6ref} \\
x_{4ref} &= -b_2 + \sqrt{\frac{b_2^2 - 4a_2 c_2}{2a_2}}
\end{aligned} \tag{4.3}$$

Although, all the references are generated initially using this technique, in the actual implementation, a combination of references obtained from this section and the virtual control references generated in the upcoming section will be utilized for maximizing the effect of back-stepping control.

4.4 Backstepping based Nonlinear Controller Design

This section delineates the detailed procedure for designing the back-stepping based controller proposed in this chapter. First, the complete mathematical design of the different controllers present in the SPVDG system is explained which is then followed by a summary of the entire procedure enumerated point-wise. The mathematical derivation of the controllers also serves as the complete stability analysis of the entire design technique. Hence, it serves a two-way purpose.

4.4.1 Controller Design Procedure:

Let us assume a Lyapunov function $V_1 = \frac{C_{pvi}}{2} e_1^2$ where $e_1 = x_1 - x_{1ref}$. Upon differentiation, we get $\dot{V}_1 = e_1(d_1 - x_3)$. If we choose x_3 as

$$\alpha_3 = d_1 + K_1 e_1 \tag{4.4}$$

then $\dot{V}_1 = -K_1 e_1^2$ which means $\dot{V}_1 < 0$. Then, we consider the Lyapunov function $V_{2,3} = \frac{C_{pvo}}{2} e_2^2 + \frac{L_{pv}}{2} e_3^2$ where, $e_2 = x_2 - x_{2ref}$ and $e_3 = x_3 - \alpha_3$. Differentiating we get,

$$\begin{aligned}\dot{V}_{2,3} &= C_{pvo} e_2 \dot{x}_2 + L_{pv} e_3 (\dot{x}_3 - \dot{\alpha}_3) \\ &= e_2 \left(x_3 + \frac{x_6 - x_2}{R_{pvo}} \right) + e_3 (x_1 - x_2 - R_{pv} x_3 - L_{pv} \dot{\alpha}_3) \\ &\quad + u_1 (-e_2 x_3 + e_3 x_2)\end{aligned}$$

If u_1 is chosen as follows:

$$u_1 = \frac{(-num_{c1} - K_2 e_2^2 - K_3 e_3^2)}{e_3 x_2 - e_2 x_3} \quad (4.5)$$

where

$$num_{c1} = e_2 x_3 - \frac{e_2 x_2}{R_{pvo}} + \frac{e_2 x_6}{R_{pvo}} + e_3 x_1 - e_3 x_2 - e_3 x_3 R_{pv} - e_3 L_{pv} \dot{\alpha}_3 \quad (4.6)$$

$$\dot{\alpha}_3 = K_1 \dot{x}_1 + \dot{d}_1 \quad (4.7)$$

then, it results in $\dot{V}_{2,3} = -K_2 e_2^2 - K_3 e_3^2$ which means $\dot{V}_{2,3} < 0$. Using this value of u_1 , the convergence of states x_1 , x_2 and x_3 of the PV array is ensured.

Now, for finding the next controller, first we choose a Lyapunov function $V_6 = \frac{C_L}{2} e_6^2$ where $e_6 = x_6 - x_{6ref}$.

$$\begin{aligned}\dot{V}_6 &= C_L e_6 \dot{x}_6 \\ &= e_6 \left[\frac{x_2}{R_{pvo}} + \frac{x_5}{R_{bo}} - x_6 \left(\frac{1}{R_{pvo}} + \frac{1}{R_{bo}} + d_3 \right) \right]\end{aligned}$$

If, the value of x_5 equals reference virtual input α_5 where

$$\alpha_5 = -\frac{R_{bo}}{R_{pvo}} x_2 + R_{bo} x_6 \left(\frac{1}{R_{pvo}} + \frac{1}{R_{bo}} + d_3 \right) - K_6 e_6 R_{bo} \quad (4.8)$$

It then becomes $\dot{V}_6 = -K_6 e_6^2$. Following this step, we choose $V_{4,5} = \frac{C_{bo}}{2} e_5^2 + \frac{L_b}{2} e_4^2$ where $e_5 = x_5 - \alpha_5$ and $e_4 = x_4 - x_{4ref}$. Upon differentiation we get,

$$\dot{V}_{4,5} = e_5 \left(x_4 - \frac{x_5}{R_{bo}} + \frac{x_4}{R_{bo}} - x_4 u_2 - C_{bo} \dot{\alpha}_5 \right) + e_4 (d_2 - x_5 - R_b x_4 + x_5 u_2) \quad (4.9)$$

We choose u_2 as follows to stabilize the system:

$$u_2 = \frac{-num_{c2} - K_4 e_4^2 - K_5 e_5^2}{e_4 x_5 - e_5 x_4} \quad (4.10)$$

where

$$num_{c2} = e_5 \left(x_4 + \frac{x_6 - x_5}{R_{bo}} - C_{bo} \dot{\alpha}_5 \right) + e_4 (d_2 - x_5 - R_b x_4) \quad (4.11)$$

$$\dot{\alpha}_5 = -\frac{R_{bo}}{R_{pvo}} \dot{x}_2 + R_{bo} x_6 \dot{d}_3 + \dot{x}_6 \left(-K_6 R_{bo} + \frac{R_{bo}}{R_{pvo}} + 1 + R_{bo} d_3 \right) \quad (4.12)$$

Then, we get, $\dot{V}_{4,5} = -K_4 e_4^2 - K_5 e_5^2$ which is equivalent to $\dot{V}_{4,5} < 0$ for $K_4, K_5 > 0$.

Thus the total Lyapunov function,

$$\dot{V} = \dot{V}_1 + \dot{V}_{2,3} + \dot{V}_{4,5} + \dot{V}_6 < 0 \quad (4.13)$$

Thus, adopting the controllers designed in (4.5), (4.10) and the virtual controllers designed in (4.4) and (4.8) which are carefully derived on the basis of Lyapunov Stability Theory, the stability of all the system states is guaranteed.

The entire procedure for designing both the MPPT and DC bus voltage controllers can be summarized in the following set of instructions.

1. Compute the reference values for all states.
2. Compute virtual input α_3 for the PV system to make x_1 follow x_{1ref} .
3. Compute the value of u_1 so that x_3 follows α_3 and x_2 follows x_{2ref} .
4. Compute the value of virtual input α_5 such that x_6 reaches its reference value x_{6ref} .
5. Compute the value of u_2 such that x_5 follows α_5 and x_4 follows its reference value x_{4ref} .

4.5 Results

In this section, different scenarios have been considered where the effects of change in irradiation, temperature and load were studied when the proposed back-stepping control is applied. The DC bus voltage is taken to be 40 V. The PV array always operates at a peak power rating of 200W. The battery operates at a constant operating voltage of 24V. The simulation has been carried out in MATLAB Table-4.1 shows gives an overall picture of various system and controller parameters used for the simulation.

Table 4.1: Parameter Specification

Subsystem	Parameter Specification
Battery Voltage	24V
PV Array at STC	Model: Kyocera Solar KC200GT $V_{OC} = 32.9V$, $I_{SC} = 8.21A$ $V_{MPP} = 26.3V$, $I_{MPP} = 7.61A$
DC/DC Converter	$C_{pvi} = 3mF$, $C_{pvo} = 3mF$, $L_{pv} = 10mH$, $R_{pv} = 0.5\Omega$, $R_{pvo} = 0.1\Omega$
DC/DC Bidirectional Converter	$C_{bo} = 3mF$, $R_b = 0.5\Omega$, $L_b = 10mH$, $R_{bo} = 0.1\Omega$
Back-stepping Gains	$K_1=10$, $K_2=0.04$, $K_3=0.04$ $K_4=0.04$, $K_5=0.04$, $K_6=15.0$

4.5.1 Case-1: Variation in Irradiance

In this case, the irradiance of PV panel is changed with time while temperature and load are kept constant at $25^\circ C$ and $200W$. The irradiance changes for every 1.5 second from $1500W/m^2$ to $1200W/m^2$ and then to $1000W/m^2$, $500W/m^2$ and $200W/m^2$ at 1.5s, 3s, 4.5s and 6s respectively. Figures 4.3 and 4.4 show the evolution of PV and battery states for this case.

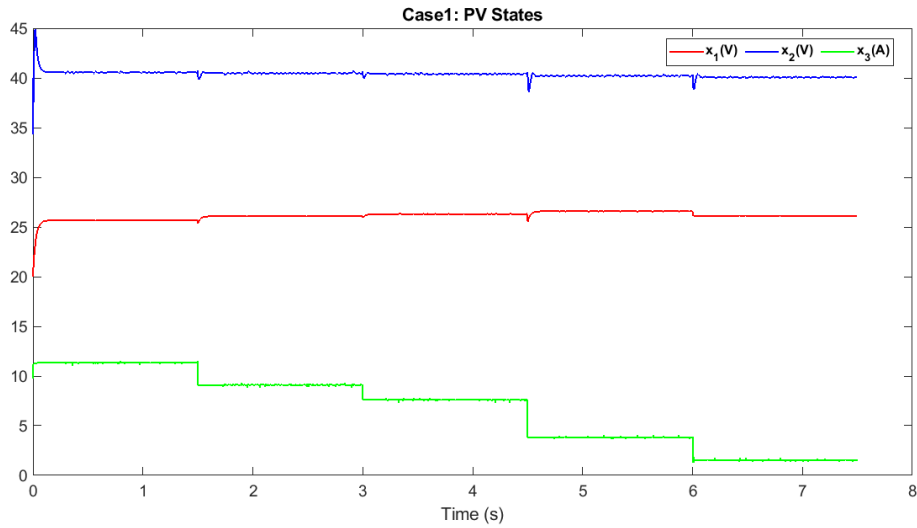


Figure 4.3: Case-1: PV states

When irradiance changes, both the voltage and current at which maximum power is extracted from the PV panel change. Moreover, the maximum power that can be extracted also reduces with reduction in irradiance. This effect is visible in the

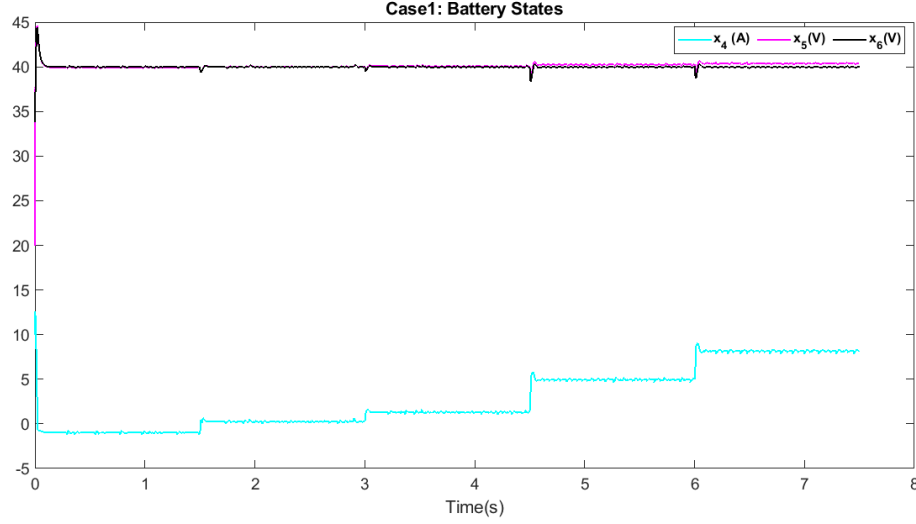


Figure 4.4: Case-1: Battery States

PV and battery currents shown in Fig.4.3. Since load is constant at $200W$, as the irradiance decreases, the PV inductor current reduces and the battery current increases compensating the reduction in PV current. During change in irradiance, some transients occur in DC bus voltage but they die out within $80ms$. Therefore, the DC bus voltage remains constant at $40V$.

4.5.2 Case-2: Variation in Temperature

With increase in temperature, the maximum power extracted from the PV panel reduces, and also the values of MPP current and voltage. In this case, the temperature is varied keeping load and irradiation constant at $200W$, $1000W/m^2$ respectively. The temperature is varied from $75^\circ C$ to $50^\circ C$ and to $25^\circ C$, $10^\circ C$ and $0^\circ C$ respectively, at $1.5s$, $3s$, $4.5s$ and $6s$ respectively.

Figures 4.5 and 4.6 show the response of the SPVDG system to change in temperature. However, the variation in MPP current extracted from PV with change in temperature is less compared to the change in MPP voltage. The grid voltage stays at $40V$ irrespective of any variation in temperature.

4.5.3 Case-3: Variation in Load

In this case, the PV panel characteristics remain constant with constant temperature and irradiation at $1000W/m^2$ and $25^\circ C$. However, the load resistance is varied from 5Ω to 7Ω , 9Ω , 11Ω and then to 8Ω at $1.5s$, $3s$, $4.5s$ and $6s$ respectively.

The change in battery current can easily be observed when PV generation is constant and load is changed. Initially, when the load is very high, the battery also supplies positive current to assuage the load requirement and gradually, as the load

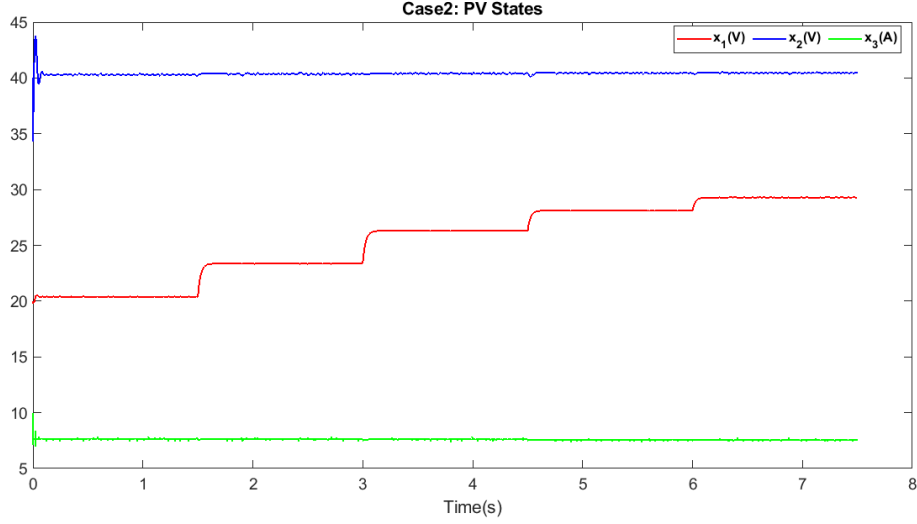


Figure 4.5: Case-2: PV states

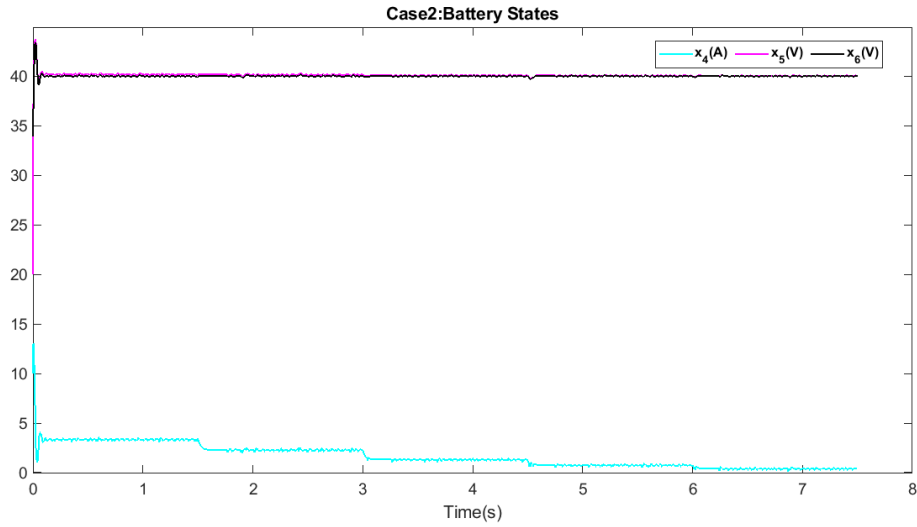


Figure 4.6: Case-2: Battery States

is reduced the current supplied by the battery reduces and when the load reduces below the maximum power provided by the PV panel, the battery current becomes negative showing that the extra power produced by the PV panel is being used to charge the battery. Its worth noting that both the MPP voltage x_1 and grid voltage x_6 remain constant.

In all the cases it can be observed that the grid is hardly perturbed without any deviations from desired value. All the states completely stabilize within $80ms$. Hence, the proposed algorithm is fast and very robust to change in disturbances.

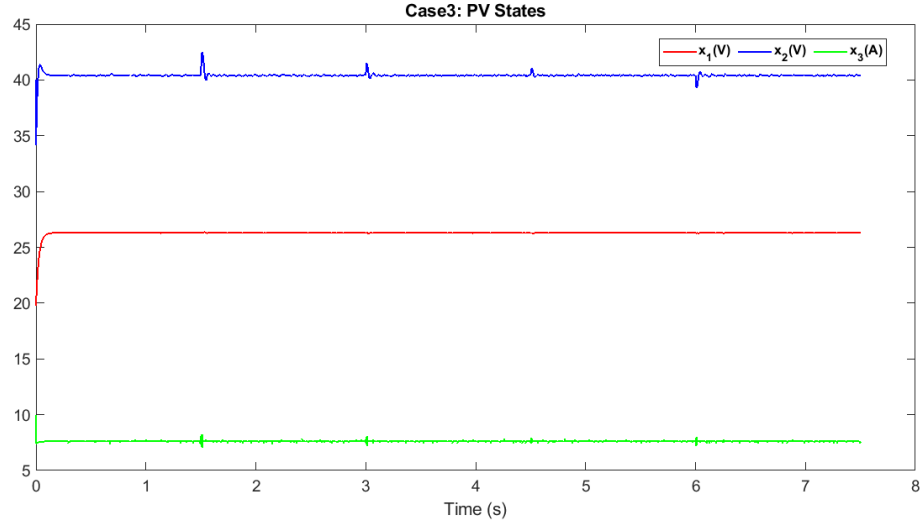


Figure 4.7: Case-3: PV states

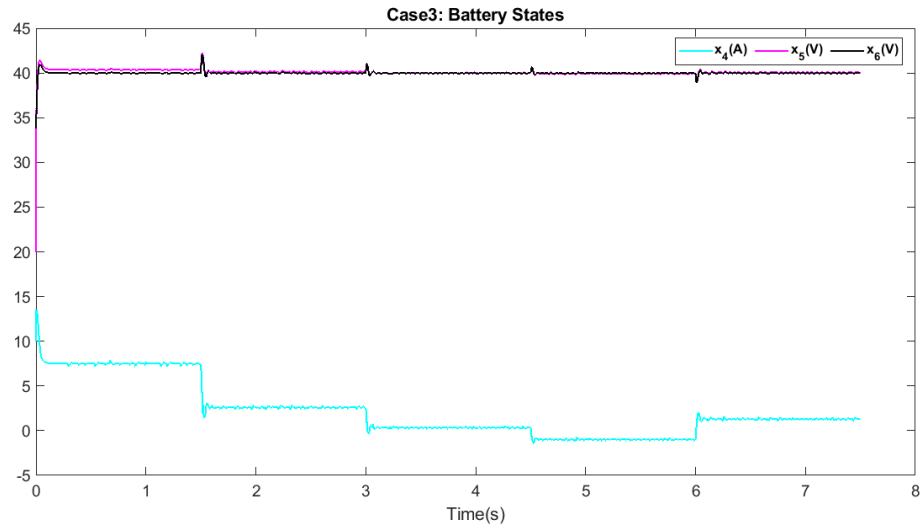


Figure 4.8: Case-3: Battery States

4.6 Summary

In this chapter, a nonlinear back-stepping control strategy is developed for a standalone PVDG system with battery energy storage. This technique ensures faster stabilization of all the system states and grid voltage when subjected to large disturbances. It has been verified for three different cases in presence of large variations in irradiance, temperature and load. This controller also ensures appropriate bidirectional power flow depending on the power balance in the standalone system. The simulation results validate the efficacy of the proposed nonlinear control strategy.

Chapter 5

Disturbance Observer based Backstepping Controller for the Isolated DCMG Unit

5.1 Introduction

In this work, the back-stepping strategy developed in the previous chapter is further equipped with disturbance observers in order to reduce the placement of excessive sensors that is demanded by the non-linear control techniques. Lyapunov stability theory is exploited to design the observers which will be clearly delineated in this chapter.

The variations in operating points during general course of operation are large due to the intermittencies in DG supply and loading conditions [75]. Therefore, it would be very difficult for these controllers to maintain stability during drastic changes like reduction in PV generation, large fluctuations in load, etc. Ensuring

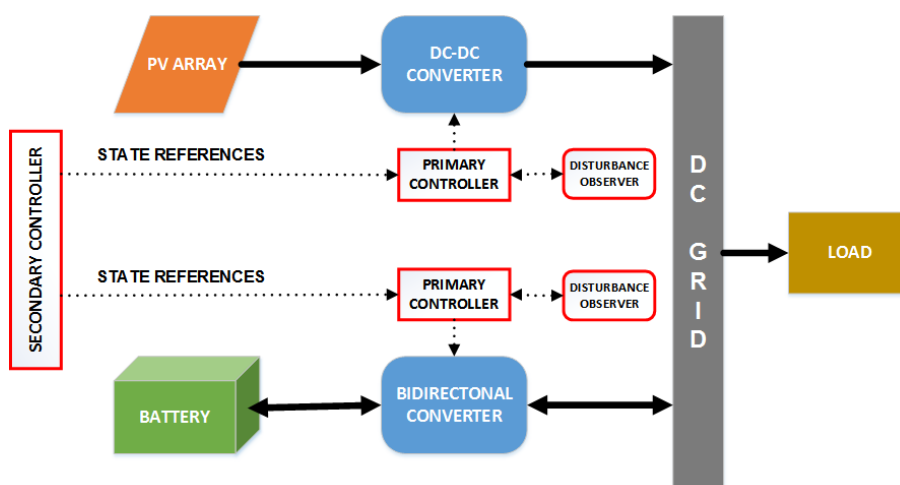


Figure 5.1: Structure of SPVDG System with observer

stability of nonlinear system models requires complex controllers to be implemented. The increase in complexity of controllers is the trade off for assuring stability inside a whole operation region.

For instance, feedback linearization, sliding mode control and adaptive control based techniques are seen to have been successfully implemented on this system in literature [76] [60]. Nevertheless, all these techniques are model-based which require continuous feedback from a lot of states and parameters existing in the system. This calls for procuring a great number of sensors for measuring these quantities for implementing them successfully. This invariably results in increasing the overall cost of the entire system. However, with the power of modern computing devices it is possible to estimate many of such parameters to feed into the nonlinear control law directly.

Works such as [77] contributed towards reducing sensors for water pumping system but these do not address MPPT or voltage control in PV based systems. A very simple technique for reducing sensors for a PV battery system was proposed in [78] which exploits the power balance of the electrical system to reduce the number of sensors in a DC microgrid but the performance of this controller was traded for making the technique cost effective. This technique will not work for large change in disturbances.

Hence, in this chapter we propose the following:

- An intuitive plug and play back-stepping based controller design for various subsystems in an islanded PV system with storage.
- An update law for observing/estimating various disturbances in the system like output current of the PV array, battery voltage and load in an online fashion.

It is also to be noted in this work that the reference values from secondary controller are readily available and hence, will mainly deal with the development of the nonlinear primary level controllers. The observers act on the same level of primary controllers and work on the basis of states' observations received from different sensors. This can be seen in Fig. 5.1.

The following is the organization of this chapter. Section 5.2 gives the complete stability proof of the disturbance observer based back-stepping control along with the designed controllers and observers. Section 5.3 shows the results that are obtained due to occurrence of different intermittencies while Section 5.4 concludes the chapter.

5.2 Disturbance Observer Based Back-stepping Controller Design

A cursory glance over the system model in (4.2) reveals that it is highly under-actuated for which back-stepping based control would be a natural choice to adopt. However, the proposed controller design technique deviates from the original process of back-stepping design since the system model doesn't exactly fit into the well-known strict-feedback structure. Moreover, it is worth noting that the disturbance observers synthesized concomitantly with the control laws were essential in the current context since it was assumed that all the disturbances are unknown. In this section, the complete process of designing the disturbance observer based back-stepping control along with its many nuances is delineated which in itself would also establish the stability of both the controllers and observers designed for the system.

Let us assume a Lyapunov function

$$W_1 = \frac{C_{pvi}}{2} e_1^2 + \frac{1}{2\rho_1} \tilde{d}_1^2 \quad (5.1)$$

where $e_1 = x_1 - x_1^d$. Taking the time derivative of W_1 we get,

$$\begin{aligned} \dot{W}_1 &= C_{pvi} e_1 \dot{e}_1 + \frac{1}{\rho_1} \tilde{d}_1 (-\dot{\tilde{d}}_1) \\ &= e_1 (d_1 - x_3) - \frac{1}{\rho_1} \tilde{d}_1 (\dot{\tilde{d}}_1) \\ &= e_1 (\tilde{d}_1 + \hat{d}_1 - x_3) - \frac{1}{\rho_1} \tilde{d}_1 (\dot{\hat{d}}_1) \\ &= e_1 (\hat{d}_1 - x_3) + \tilde{d}_1 (e_1 - \frac{\dot{\hat{d}}_1}{\rho_1}) \end{aligned} \quad (5.2)$$

We choose the values of x_3 to be equal to α_3 and $\dot{\hat{d}}_1$ as follows:

$$\begin{aligned} \alpha_3 &= \hat{d}_1 + K_1 e_1 \\ \dot{\hat{d}}_1 &= \rho_1 e_1 \end{aligned} \quad (5.3)$$

Substituting these values, we get $\dot{W}_1 = -K_1 e_1^2$. Assuming $K_1 > 0$, it can be concluded that $\dot{W}_1 < 0$

Now considering $e_2 = x_2 - x_2^d$ and $e_3 = x_3 - \alpha_3$, we define the following Lyapunov function jointly for the second and third states:

$$\begin{aligned} W_{2,3} &= \frac{C_{pvo}}{2} e_2^2 + \frac{L_{pv}}{2} e_3^2 \\ \dot{W}_{2,3} &= C_{pvo} e_2 \dot{e}_2 + L_{pv} e_3 (\dot{x}_3 - \dot{\alpha}_3) \end{aligned} \quad (5.4)$$

Upon rearranging different terms, $\dot{W}_{2,3}$ becomes as follows:

$$\begin{aligned}\dot{W}_{2,3} &= e_2\left(x_3 + \frac{x_6 - x_2}{R_{pvo}}\right) + e_3(x_1 - x_2 - R_{pv}x_3) \\ &\quad + u_1(e_3x_2 - e_2x_3)\end{aligned}$$

We choose u_1 as follows:

$$\begin{aligned}num_{c1} &= e_2\left(x_3 + \frac{x_6 - x_2}{R_{pvo}}\right) + e_3(x_1 - x_2 - R_{pv}x_3) \\ den_{c1} &= e_3x_2 - e_2x_3 \\ u_1 &= \frac{-K_2e_2^2 - K_3e_3^2 - num_{c1}}{den_{c1}}\end{aligned}\tag{5.5}$$

Thus, we get $\dot{W}_{2,3} = -K_2e_2^2 - K_3e_3^2$ which is equivalent to $\dot{W}_{2,3} < 0$ for $K_2, K_3 > 0$.

The next Lyapunov function is assumed as follows:

$$W_6 = \frac{C_L}{2}e_6^2 + \frac{1}{2\rho_3}\tilde{d}_3^2\tag{5.6}$$

Differentiating this function we get,

$$\begin{aligned}\dot{W}_6 &= e_6\left[\frac{x_2}{R_{pvo}} + \frac{x_5}{R_{bo}} - x_6\left(\frac{1}{R_{pvo}} + \frac{1}{R_{bo}} + \hat{d}_3\right)\right] \\ &\quad - \tilde{d}_3\left[\frac{\dot{\hat{d}}_3}{\rho_3} + x_6e_6\right]\end{aligned}\tag{5.7}$$

Choosing x_5 to be α_5 and $\dot{\hat{d}}_3$ as follows:

$$\begin{aligned}\alpha_5 &= -R_{bo}K_6e_6 + R_{bo}x_6\left(\frac{1}{R_{pvo}} + \frac{1}{R_{bo}} + \hat{d}_3\right) - \frac{R_{bo}}{R_{pvo}}x_2 \\ \dot{\hat{d}}_3 &= -\rho_3x_6e_6\end{aligned}\tag{5.8}$$

we get $\dot{W}_6 = -K_6e_6^2 < 0$ if $K_6 > 0$. For designing u_2 , the final Lyapunov function is chosen as follows:

$$W_{4,5} = \frac{L_b}{2}e_4^2 + \frac{C_{bo}}{2}e_5^2 + \frac{1}{2\rho_2}\tilde{d}_2^2$$

where $e_4 = x_4 - x_4^d$ and $e_5 = x_5 - \alpha_5$ Taking the derivative,

$$\dot{W}_{4,5} = L_be_4\dot{x}_4 + C_{bo}e_5(\dot{x}_5 - \dot{\alpha}_5) + \frac{1}{\rho_2}\tilde{d}_2(-\dot{\hat{d}}_2)\tag{5.9}$$

Substituting and rearranging the terms, we get,

$$\begin{aligned}\dot{W}_{4,5} = & e_4(\hat{d}_2 - x_5 - R_b x_4) + e_5(x_4 + \frac{x_6 - x_5}{R_{bo}}) \\ & - e_5(x_4 u_2 + C_{bo} \dot{\alpha}_5) + \tilde{d}_2(e_4 - \frac{\dot{\hat{d}}_2}{\rho_2})\end{aligned}\quad (5.10)$$

By choosing the following,

$$\begin{aligned}num_{c2} &= -e_4(\hat{d}_2 - x_5 - R_b x_4) - e_5 x_4 \\ &\quad - e_5(\frac{x_6 - x_5}{R_{bo}} - C_{bo} \dot{\alpha}_5) \\ den_{c2} &= e_4 x_5 - e_5 x_4 \\ u_2 &= \frac{num_{c2} - K_5 e_5^2 - K_6 e_6^2}{den_{c2}}\end{aligned}\quad (5.11)$$

$$\hat{d}_2 = \rho_2 e_4 \quad (5.12)$$

we get, $\dot{W}_{4,5} = -K_4 e_4^2 - K_5 e_5^2$ which is equivalent to $\dot{W}_{4,5} < 0$ for $K_4, K_5 > 0$. Thus the total Lyapunov function,

$$\dot{W} = \dot{W}_1 + \dot{W}_{2,3} + \dot{W}_{4,5} + \dot{W}_6 < 0 \quad (5.13)$$

Thus, adopting the controllers designed in (5.5), (5.11) and the estimation update laws in (5.3), (5.12) and (5.8), stability of all the states and disturbance observers is guaranteed.

5.3 Simulation Results

In this section, three different cases are investigated related to the change in different external disturbances like temperature, irradiation and load to validate the effectiveness of the proposed disturbance observer based back-stepping control strategy. The DC bus voltage of the SPVDG system is chosen to be 40V. The PV system has a peak power rating of 200W at standard temperature and irradiance and the load fluctuates between 145W and 320W. It is also to be noted that in this work, the PV is always operated at maximum power. Table-5.1 shows the specifications of the various components used in the SPVDG system along with the controller and observer gains used to implement the proposed technique. It is to be noted that all the simulations were carried out in the MATLAB environment.

It is clearly visible from figures 5.3, 5.5 and 5.7 that the disturbance observers start at a random value and update their values in an online fashion leading to simultaneous stabilization of the states by the controllers. The observers continuously

monitor the different states and accordingly update their values such that desired control is achieved.

Table 5.1: Parameter Specification

Subsystem	Parameter Specification
Battery Voltage	24V
PV Array at STC	Model: Kyocera Solar KC200GT $V_{OC} = 32.9V$, $I_{SC} = 8.21A$ $V_{MPP} = 26.3V$, $I_{MPP} = 7.61A$
DC/DC Converter	$C_{pvi} = 3mF$, $C_{pvo} = 3mF$, $L_{pv} = 10mH$, $R_{pv} = 0.5\Omega$, $R_{pvo} = 0.1\Omega$
DC/DC Bidirectional Converter	$C_{bo} = 3mF$, $R_b = 0.5\Omega$, $L_b = 10mH$, $R_{bo} = 0.1\Omega$
Back-stepping Gains	$K_1=17$, $K_2=0.04$, $K_3=0.04$ $K_4=0.06$, $K_5=0.06$, $K_6=19.0$
Observer Gains	$\gamma_1=10$, $\gamma_3=0.01$

5.3.1 Case-1: Change in Irradiance

In this case, the irradiance of PV panel is changed with time while temperature and load are kept constant at 25°C and 200W. The irradiance changes for every 1.5 second from 1500W/m² to 1200W/m² and then to 1000W/m², 500W/m² and 200W/m² at 1.5s, 3s, 4.5s and 6s respectively. Figures 5.2 and 5.3 show the evolution of pertinent states and estimated disturbance values in this case.

When irradiance changes, both the voltage and current at which maximum power is extracted from the PV panel change. Moreover, the maximum power that can be extracted also reduces with reduction in irradiance. This effect is visible in the PV and battery currents shown in Fig.5.2. Since load is constant at 200W, as the irradiance decreases, the PV inductor current reduces and the battery current increases compensating the reduction in PV current. During change in irradiance, some transients occur in DC bus voltage but they die out within 100ms. Therefore, the DC bus voltage remains constant at 40V.

5.3.2 Case-2: Change in Temperature

With increase in temperature, the maximum power extracted from the PV panel reduces, and also the values of MPP current and voltage. In this case, the temperature

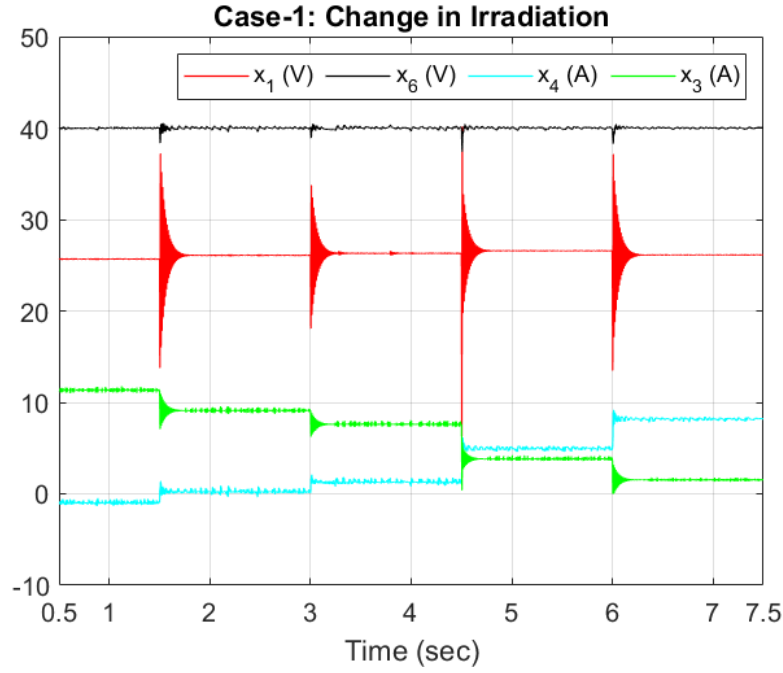


Figure 5.2: Case-1: Relevant states

is varied keeping load and irradiation constant at $266.7W$, $1000W/m^2$ respectively. The temperature is varied from $75^\circ C$ to $50^\circ C$ and to $25^\circ C$, $10^\circ C$ and $0^\circ C$ respectively, at $1.5s$, $3s$, $4.5s$ and $6s$ respectively.

Figures 5.4 and 5.5 show the response of the SPVDG system to change in temperature and the estimation of disturbance d_1 respectively. However, the variation in MPP current extracted from PV with change in temperature is less compared to the change in MPP voltage. The grid voltage stays at $40V$ irrespective of any variation in temperature.

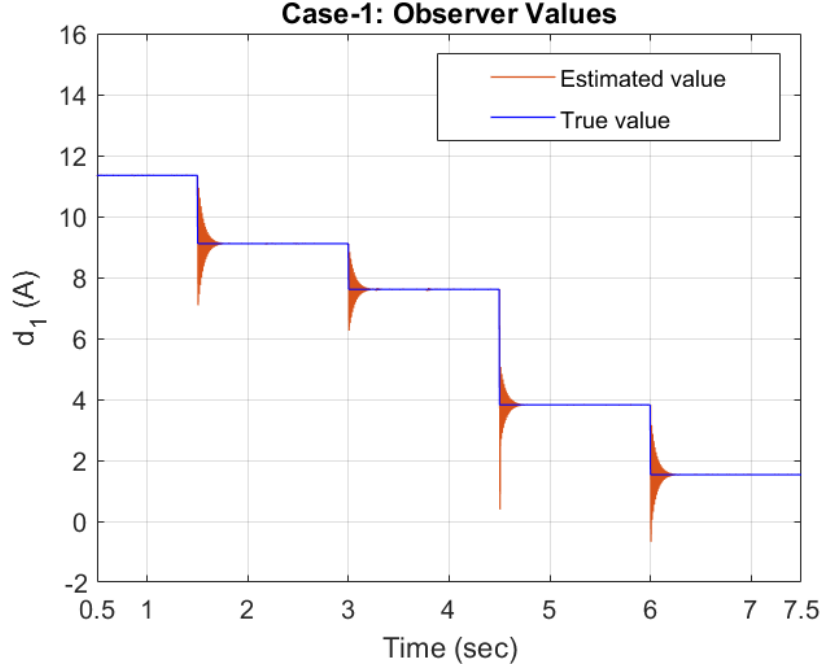


Figure 5.3: Case-1: Observer values

5.3.3 Case-3: Change in Load

In this case, the PV panel characteristics remain constant with constant temperature and irradiation at $1000W/m^2$ and $25^\circ C$. However, the load resistance is varied from 5Ω to 7Ω , 9Ω , 11Ω and then to 8Ω at $1.5s$, $3s$, $4.5s$ and $6s$ respectively.

The change in battery current can easily be observed when PV generation is constant and load is changed. Initially, when the load is very high, the battery also supplies positive current to assuage the load requirement and gradually, as the load is reduced the current supplied by the battery reduces and when the load reduces below the maximum power provided by the PV panel, the battery current becomes negative showing that the extra power produced by the PV panel is being used to charge the battery. Its worth noting that both the MPP voltage x_1 and grid voltage x_6 remain constant.

In all the cases it can be observed that the grid is hardly perturbed without any deviations from desired value. All the other states and disturbance estimators completely stabilize within $100ms$. In case-3, it is found that although the disturbance estimation is slower for some variations in load, the DC bus voltage control performance is not affected. Hence, the proposed algorithm is not only fast but also very robust to change in disturbances.

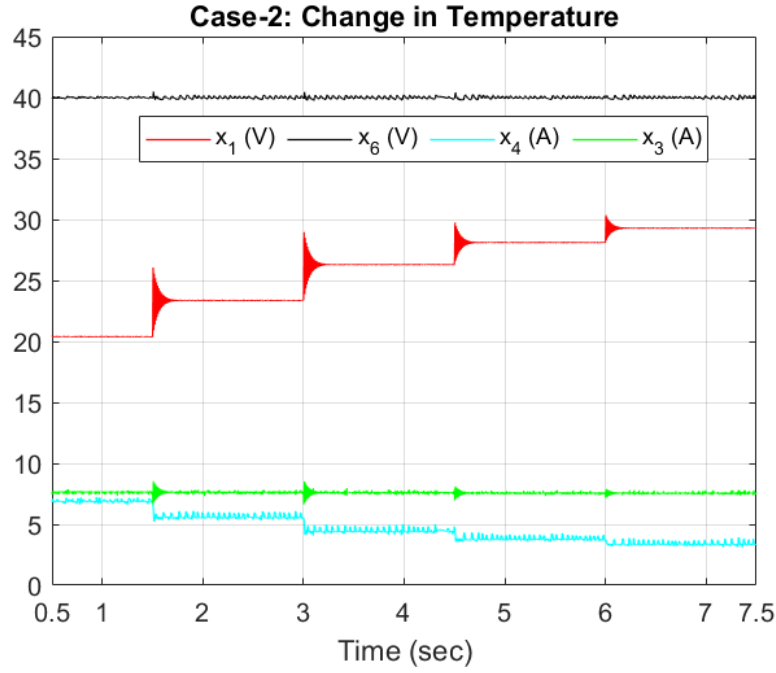


Figure 5.4: Case-2: Relevant states

5.4 Summary

In this chapter, a disturbance observer based back-stepping control strategy is developed for a standalone PVDG system with battery energy storage. This technique ensures elimination of sensors for measuring PV array output current and load current while preserving all the positive effects of non-linear model based control. The back-stepping controller designed in this chapter results in faster MPP tracking and voltage control. It has been verified for three different cases in presence of intermittencies in irradiance, temperature and load. This controller also ensures appropriate bidirectional power flow depending on the power balance in the standalone system. The simulation results validate the efficacy of the proposed nonlinear control strategy with reduced sensor count resulting in lower system cost while providing better performance.

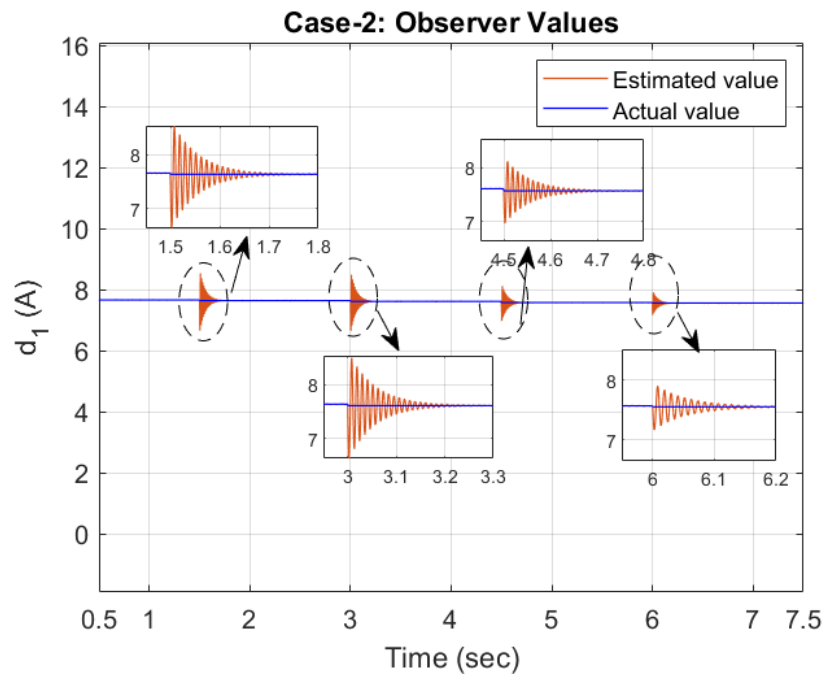


Figure 5.5: Case-2: Observer values

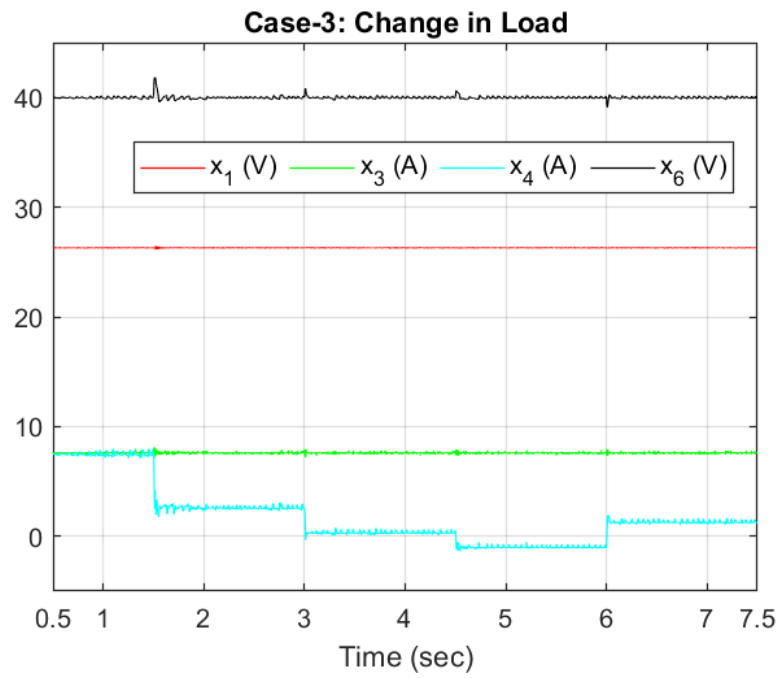


Figure 5.6: Case-3: Relevant states

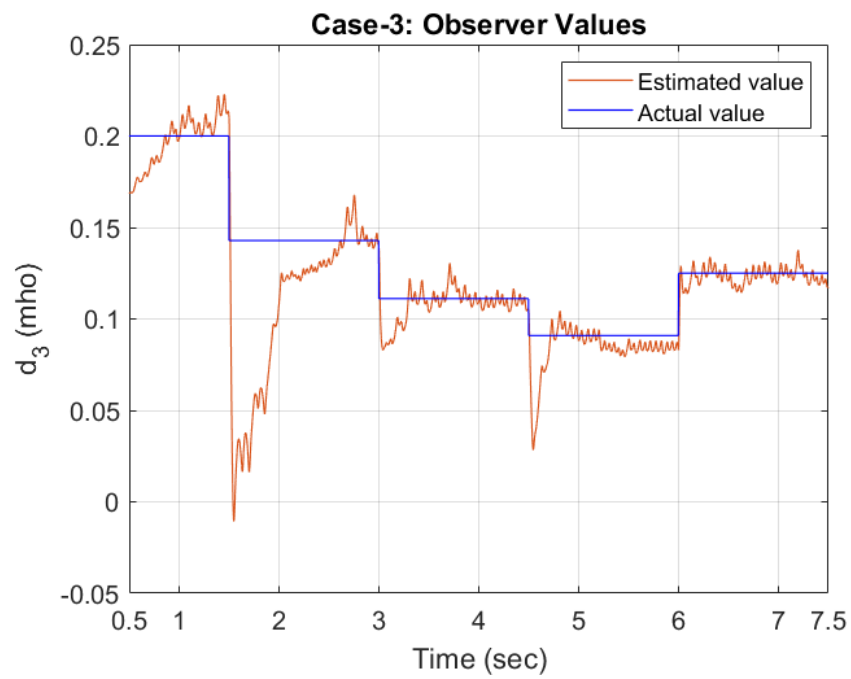


Figure 5.7: Case-3: Observer values

Chapter 6

Conclusion and Future Scope

6.1 Conclusion

In this thesis, we have developed many techniques mainly with a motivation to achieve two objectives :

- To reduce the number of sensors used in SPVDG system which contributes towards lesser cost of the overall system.
- To make the SPVDG system more flexible in the sense that it can work in extended ranges of operation while maintaining good performance when subjected to large and sudden disturbances from load and atmospheric conditions.

The second chapter discusses a methodology to estimate ambient temperature and irradiation whose data can be used to develop single-step MPPT techniques for PV arrays based on model estimation. When this technique is coupled with a suitable nonlinear control technique, it is possible to achieve MPPT in a record time of 200ms even for drastic changes in atmospheric conditions. In chapter three, we explore a low computation based technique to reduce the sensor requirement in SPVDG systems. We see that when this technique is used, for small changes in irradiation and temperature the MPPT time is around 200ms and voltage control takes around 100ms. However, this method requires the use of linear controllers whose operational range is very low and this technique cannot tolerate heavy disturbances. Hence, in the fourth chapter, we develop a nonlinear back-stepping based controller so that both operational range is enhanced and speed is also maintained. It is seen that it is possible to stabilize the system states around 80ms even in case of large disturbances. But this technique again uses too many sensors and thus, in the fifth, chapter we propose a disturbance observer based strategy to overcome the extreme sensor requirement issue in back-stepping controller. This technique was seen to stabilize all the system states and observer values around 100ms which makes it

very much viable to implement on SPVDG systems with less sensors and improved performance.

6.2 Future Scope

The work done in this thesis has a lot of potential to be carried forward. Some of the future directions are enumerated as follows:

- The thesis considers only resistive load for evaluating the algorithms. All the algorithms can be expanded to more practical loads like constant power load, AC loads.
- The algorithms and controllers developed in this thesis can be applied to a much bigger DC system with varied renewable sources like wind, fuel cell and also in the presence of a diesel generator for emergency situations.
- All the works developed in this thesis consider only an isolated PVDG system. Such issues can be explored also in the grid-connected scenario.
- As we advance towards more adaptive and disturbance observer based techniques where system information is low, it is difficult to compute the secondary level references. Hence, learning based secondary level reference generation can be explored.
- The system must be tested using stochastic disturbances after sufficient modeling of the disturbance data.

List of Publications

1. A. Hussain, M. M. Garg, M. P. Korukonda, S. Hasan and L. Behera, "A Parameter Estimation Based MPPT Method for a PV System Using Lyapunov Control Scheme," in IEEE Transactions on Sustainable Energy, vol. 10, no. 4, pp. 2123-2132, Oct. 2019.
2. M. Satapathy, M. P. Korukonda, A. Hussain and L. Behera, "A Direct Perturbation based Sensor-free MPPT with DC Bus Voltage Control for a Standalone DC Microgrid," 2019 IEEE PES Innovative Smart Grid Technologies Europe (ISGT-Europe), Bucharest, Romania, 2019, pp. 1-5.
3. M.P.Korukonda, M.M Garg, A. Hussain and L.Behera, "Disturbance Observer based Controller Design to Reduce Sensor Count in Standalone PVDG Systems", (Submitted to IECON-2020, Singapore)

Bibliography

- [1] J. T. Bialasiewicz, “Renewable energy systems with photovoltaic power generators: Operation and modeling,” *IEEE Transactions on Industrial Electronics*, vol. 55, no. 7, pp. 2752–2758, 2008.
- [2] J. Xiao, L. Bai, F. Li, H. Liang, and C. Wang, “Sizing of energy storage and diesel generators in an isolated microgrid using discrete fourier transform (dft),” *IEEE Transactions on Sustainable Energy*, vol. 5, no. 3, pp. 907–916, 2014.
- [3] T. V. Thang, A. Ahmed, C. Kim, and J. Park, “Flexible system architecture of stand-alone pv power generation with energy storage device,” *IEEE Transactions on Energy Conversion*, vol. 30, no. 4, pp. 1386–1396, 2015.
- [4] R. Panigrahi, S. Mishra, S. C. Srivastava, A. K. Srivastava, and N. Schulz, “Grid integration of small-scale photovoltaic systems in secondary distribution network- a review,” *IEEE Transactions on Industry Applications*, pp. 1–1, 2020.
- [5] T. K. Roy, M. A. Mahmud, A. M. T. Oo, M. E. Haque, K. M. Muttaqi, and N. Mendis, “Nonlinear adaptive backstepping controller design for islanded dc microgrids,” *IEEE Transactions on Industry Applications*, vol. 54, no. 3, pp. 2857–2873, 2018.
- [6] V. Nasirian, A. Davoudi, F. L. Lewis, and J. M. Guerrero, “Distributed adaptive droop control for dc distribution systems,” *IEEE Transactions on Energy Conversion*, vol. 29, no. 4, pp. 944–956, 2014.
- [7] T. K. Roy and M. A. Mahmud, “Dynamic stability analysis of hybrid islanded dc microgrids using a nonlinear backstepping approach,” *IEEE Systems Journal*, vol. 12, no. 4, pp. 3120–3130, 2018.
- [8] J. Xiao, P. Wang, and L. Setyawan, “Multilevel energy management system for hybridization of energy storages in dc microgrids,” *IEEE Transactions on Smart Grid*, vol. 7, no. 2, pp. 847–856, 2016.

- [9] T. V. Thang, A. Ahmed, C. Kim, and J. Park, “Flexible system architecture of stand-alone pv power generation with energy storage device,” *IEEE Transactions on Energy Conversion*, vol. 30, no. 4, pp. 1386–1396, 2015.
- [10] A. Hussain, M. M. Garg, M. P. Korukonda, S. Hasan, and L. Behera, “A parameter estimation based mppt method for a pv system using lyapunov control scheme,” *IEEE Transactions on Sustainable Energy*, vol. 10, no. 4, pp. 2123–2132, 2019.
- [11] S. Augustine, M. K. Mishra, and N. Lakshminarasamma, “A unified control scheme for a standalone solar-pv lvdc microgrid system with hess,” *IEEE Journal of Emerging and Selected Topics in Power Electronics*, pp. 1–1, 2019.
- [12] Y. Yang, Y. Qin, S. Tan, and S. Y. R. Hui, “Efficient improvement of photovoltaic-battery systems in standalone dc microgrids using a local hierarchical control for the battery system,” *IEEE Transactions on Power Electronics*, vol. 34, no. 11, pp. 10796–10807, 2019.
- [13] R. R. Deshmukh, M. S. Ballal, H. M. Suryawanshi, and M. K. Mishra, “An adaptive approach for effective power management in dc microgrid based on virtual generation in distributed energy sources,” *IEEE Transactions on Industrial Informatics*, vol. 16, no. 1, pp. 362–372, 2020.
- [14] M. P. Korukonda, S. R. Mishra, K. Rajawat, and L. Behera, “Hybrid adaptive framework for coordinated control of distributed generators in cyber-physical energy systems,” *IET Cyber-Physical Systems: Theory Applications*, vol. 3, no. 1, pp. 54–62, 2018.
- [15] M. P. Korukonda, S. R. Mishra, A. Shukla, and L. Behera, “Handling multi-parametric variations in distributed control of cyber-physical energy systems through optimal communication design,” *IET Cyber-Physical Systems: Theory Applications*, vol. 2, no. 2, pp. 90–100, 2017.
- [16] S. R. Mishra, N. V. Srinath, K. M. Preetam, and L. Behera, “A generalized novel framework for optimal sensor-controller connection design to guarantee a stable cyber physical smart grid,” in *2015 IEEE 13th International Conference on Industrial Informatics (INDIN)*, 2015, pp. 424–429.
- [17] S. R. Mishra, M. P. Korukonda, L. Behera, and A. Shukla, “Enabling cyber-physical demand response in smart grids via conjoint communication and controller design,” *IET Cyber-Physical Systems: Theory Applications*, vol. 4, no. 4, pp. 291–303, 2019.

- [18] M. P. Korukonda, S. R. Mishra, A. Shukla, and L. Behera, "Improving micro-grid voltage stability through cyber-physical control," in *2016 National Power Systems Conference (NPSC)*, 2016, pp. 1–6.
- [19] Anuj Nandanwar, Meher Preetam Korukonda, and Laxmidhar Behera, "A routing scheme for voltage stabilization in cyber physical energy systems," *IFAC Proceedings Volumes*, vol. 47, no. 1, pp. 812 – 818, 2014, 3rd International Conference on Advances in Control and Optimization of Dynamical Systems (2014).
- [20] A. M. Betti, M. A. Ebrahim, and M. A. Mustafa Hassan, "Modeling and control of stand-alone pv system based on fractional-order pid controller," in *2018 Twentieth International Middle East Power Systems Conference (MEPCON)*, 2018, pp. 377–382.
- [21] V. Karthikeyan and R. Gupta, "Varying phase angle control in isolated bidirectional dc/dc converter for integrating battery storage and solar pv system in standalone mode," *IET Power Electronics*, vol. 10, no. 4, pp. 471–479, 2017.
- [22] S. Strache, R. Wunderlich, and S. Heinen, "A comprehensive, quantitative comparison of inverter architectures for various pv systems, pv cells, and irradiance profiles," *IEEE Transactions on Sustainable Energy*, vol. 5, no. 3, pp. 813–822, 2014.
- [23] A. K. S. Bhat and S. B. Dewan, "A novel utility interfaced high-frequency link photovoltaic power conditioning system," *IEEE Transactions on Industrial Electronics*, vol. 35, no. 1, pp. 153–159, 1988.
- [24] S. M. Alghuwainem, "Speed control of a pv powered dc motor driving a self-excited 3-phase induction generator for maximum utilization efficiency," *IEEE Transactions on Energy Conversion*, vol. 11, no. 4, pp. 768–773, 1996.
- [25] E. Romero-Cadaval, G. Spagnuolo, L. G. Franquelo, C. A. Ramos-Paja, T. Suntio, and W. M. Xiao, "Grid-connected photovoltaic generation plants: Components and operation," *IEEE Industrial Electronics Magazine*, vol. 7, no. 3, pp. 6–20, 2013.
- [26] Juan David Bastidas-Rodriguez, "Maximum power point tracking architectures for photovoltaic systems in mismatching conditions: a review," *IET Power Electronics*, vol. 7, pp. 1396–1413(17), June 2014.
- [27] A Pallavee Bhatnagar and BRK Nema, "Conventional and global maximum power point tracking techniques in photovoltaic applications: A review," *Journal of Renewable and Sustainable Energy*, vol. 5, no. 3, pp. 032701, 2013.

- [28] B. Subudhi and R. Pradhan, "A comparative study on maximum power point tracking techniques for photovoltaic power systems," *IEEE Transactions on Sustainable Energy*, vol. 4, no. 1, pp. 89–98, 2013.
- [29] N. Femia, D. Granozio, G. Petrone, G. Spagnuolo, and M. Vitelli, "Predictive adaptive mppt perturb and observe method," *IEEE Transactions on Aerospace and Electronic Systems*, vol. 43, no. 3, pp. 934–950, 2007.
- [30] N. Femia, G. Petrone, G. Spagnuolo, and M. Vitelli, "Optimization of perturb and observe maximum power point tracking method," *IEEE Transactions on Power Electronics*, vol. 20, no. 4, pp. 963–973, 2005.
- [31] M. A. Elgendy, B. Zahawi, and D. J. Atkinson, "Assessment of the incremental conductance maximum power point tracking algorithm," *IEEE Transactions on Sustainable Energy*, vol. 4, no. 1, pp. 108–117, 2013.
- [32] Nahla E. Zakzouk, "Improved performance low-cost incremental conductance pv mppt technique," *IET Renewable Power Generation*, vol. 10, pp. 561–574(13), April 2016.
- [33] M. Adly, H. El-Sherif, and M. Ibrahim, "Maximum power point tracker for a pv cell using a fuzzy agent adapted by the fractional open circuit voltage technique," in *2011 IEEE International Conference on Fuzzy Systems (FUZZ-IEEE 2011)*, 2011, pp. 1918–1922.
- [34] A. Sandali, T. Oukhoya, and A. Cheriti, "Modeling and design of pv grid connected system using a modified fractional short-circuit current mppt," in *2014 International Renewable and Sustainable Energy Conference (IRSEC)*, 2014, pp. 224–229.
- [35] T. Esum, J. W. Kimball, P. T. Krein, P. L. Chapman, and P. Midya, "Dynamic maximum power point tracking of photovoltaic arrays using ripple correlation control," *IEEE Transactions on Power Electronics*, vol. 21, no. 5, pp. 1282–1291, 2006.
- [36] M. Rakhshan, N. Vafamand, M. Khooban, and F. Blaabjerg, "Maximum power point tracking control of photovoltaic systems: A polynomial fuzzy model-based approach," *IEEE Journal of Emerging and Selected Topics in Power Electronics*, vol. 6, no. 1, pp. 292–299, 2018.
- [37] Muhammad Ammirul Atiqi Mohd Zainuri, "Development of adaptive perturb and observe-fuzzy control maximum power point tracking for photovoltaic boost dc/dc converter," *IET Renewable Power Generation*, vol. 8, pp. 183–194(11), March 2014.

- [38] K. L. Lian, J. H. Jhang, and I. S. Tian, "A maximum power point tracking method based on perturb-and-observe combined with particle swarm optimization," *IEEE Journal of Photovoltaics*, vol. 4, no. 2, pp. 626–633, 2014.
- [39] K. Ishaque, Z. Salam, M. Amjad, and S. Mekhilef, "An improved particle swarm optimization (psa)based mppt for pv with reduced steady-state oscillation," *IEEE Transactions on Power Electronics*, vol. 27, no. 8, pp. 3627–3638, 2012.
- [40] L. M. Elobaid, A. K. Abdelsalam, and E. E. Zakzouk, "Artificial neural network-based photovoltaic maximum power point tracking techniques: a survey," *IET Renewable Power Generation*, vol. 9, no. 8, pp. 1043–1063, 2015.
- [41] Yousra Shaiek, Mouna [Ben Smida], Anis Sakly, and Mohamed Faouzi Mimouni, "Comparison between conventional methods and ga approach for maximum power point tracking of shaded solar pv generators," *Solar Energy*, vol. 90, pp. 107 – 122, 2013.
- [42] A. A. Elbaset, H. Ali, M. Abd-El Sattar, and M. Khaled, "Implementation of a modified perturb and observe maximum power point tracking algorithm for photovoltaic system using an embedded microcontroller," *IET Renewable Power Generation*, vol. 10, no. 4, pp. 551–560, 2016.
- [43] F. Liu, S. Duan, F. Liu, B. Liu, and Y. Kang, "A variable step size inc mppt method for pv systems," *IEEE Transactions on Industrial Electronics*, vol. 55, no. 7, pp. 2622–2628, 2008.
- [44] T. K. Soon and S. Mekhilef, "A fast-converging mppt technique for photovoltaic system under fast-varying solar irradiation and load resistance," *IEEE Transactions on Industrial Informatics*, vol. 11, no. 1, pp. 176–186, 2015.
- [45] L. M. Elobaid, A. K. Abdelsalam, and E. E. Zakzouk, "Artificial neural network-based photovoltaic maximum power point tracking techniques: a survey," *IET Renewable Power Generation*, vol. 9, no. 8, pp. 1043–1063, 2015.
- [46] E. I. Batzelis, G. E. Kampitsis, S. A. Papathanassiou, and S. N. Manias, "Direct mpp calculation in terms of the single-diode pv model parameters," *IEEE Transactions on Energy Conversion*, vol. 30, no. 1, pp. 226–236, 2015.
- [47] H. Abu-Rub, A. Iqbal, S. Moin Ahmed, F. Z. Peng, Y. Li, and G. Baoming, "Quasi-z-source inverter-based photovoltaic generation system with maximum power tracking control using anfis," *IEEE Transactions on Sustainable Energy*, vol. 4, no. 1, pp. 11–20, 2013.

- [48] M. G. Villalva, J. R. Gazoli, and E. R. Filho, “Comprehensive approach to modeling and simulation of photovoltaic arrays,” *IEEE Transactions on Power Electronics*, vol. 24, no. 5, pp. 1198–1208, 2009.
- [49] S. Kumar, H. S. Sahu, and S. K. Nayak, “Estimation of mpp of a double diode model pv module from explicit iv characteristic,” *IEEE Transactions on Industrial Electronics*, vol. 66, no. 9, pp. 7032–7042, 2019.
- [50] M. Haouari-Merbah, M. Belhamel, I. Tobas, and J.M. Ruiz, “Extraction and analysis of solar cell parameters from the illuminated current-voltage curve,” *Solar Energy Materials and Solar Cells*, vol. 87, no. 1, pp. 225 – 233, 2005, International Conference on Physics, Chemistry and Engineering.
- [51] Jen-Cheng Wang, Yu-Li Su, Jyh-Cherng Shieh, and Joe-Air Jiang, “High-accuracy maximum power point estimation for photovoltaic arrays,” *Solar Energy Materials and Solar Cells*, vol. 95, no. 3, pp. 843 – 851, 2011.
- [52] J. J. Soon and K. Low, “Photovoltaic model identification using particle swarm optimization with inverse barrier constraint,” *IEEE Transactions on Power Electronics*, vol. 27, no. 9, pp. 3975–3983, 2012.
- [53] Y. Mahmoud, M. Abdelwahed, and E. F. El-Saadany, “An enhanced mppt method combining model-based and heuristic techniques,” *IEEE Transactions on Sustainable Energy*, vol. 7, no. 2, pp. 576–585, 2016.
- [54] M. Jedari Zare Zadeh and S. H. Fathi, “A new approach for photovoltaic arrays modeling and maximum power point estimation in real operating conditions,” *IEEE Transactions on Industrial Electronics*, vol. 64, no. 12, pp. 9334–9343, 2017.
- [55] N. Femia, G. Petrone, G. Spagnuolo, and M. Vitelli, *Power Electronics and Control Techniques for Maximum Energy Harvesting in Photovoltaic Systems*, Industrial Electronics. CRC Press, 2017.
- [56] A. Ahmed, L. Ran, S. Moon, and J. Park, “A fast pv power tracking control algorithm with reduced power mode,” *IEEE Transactions on Energy Conversion*, vol. 28, no. 3, pp. 565–575, 2013.
- [57] U. Jadli, P. Thakur, and R. D. Shukla, “A new parameter estimation method of solar photovoltaic,” *IEEE Journal of Photovoltaics*, vol. 8, no. 1, pp. 239–247, 2018.

- [58] W. [De Soto], S.A. Klein, and W.A. Beckman, "Improvement and validation of a model for photovoltaic array performance," *Solar Energy*, vol. 80, no. 1, pp. 78 – 88, 2006.
- [59] R. Haroun, A. El Aroudi, A. Cid-Pastor, G. Garcia, C. Olalla, and L. Martinez-Salamero, "Impedance matching in photovoltaic systems using cascaded boost converters and sliding-mode control," *IEEE Transactions on Power Electronics*, vol. 30, no. 6, pp. 3185–3199, 2015.
- [60] A. Hussain, A. Kumar, and L. Behera, "Sliding mode control of a buck converter for maximum power point tracking of a solar panel," in *2013 IEEE International Conference on Control Applications (CCA)*, 2013, pp. 661–666.
- [61] D. Chen and L. Xu, "Autonomous dc voltage control of a dc microgrid with multiple slack terminals," *IEEE Transactions on Power Systems*, vol. 27, no. 4, pp. 1897–1905, Nov 2012.
- [62] M. V. G. Varaprasad and S. Maity, "Development of current sensorless photovoltaic mpp tracker," in *2019 International Conference on Computer, Electrical Communication Engineering (ICCECE)*, 2019, pp. 1–5.
- [63] Xiang-Dong Sun, M. Matsui, and Kouji Yanagimura, "Novel single-voltage-sensor-based maximum power point tracking method," in *2007 7th International Conference on Power Electronics*, 2007, pp. 847–850.
- [64] A. Agrawal and R. Gupta, "Single sensor based ess controller for dc bus stabilization in low power isolated solar pv system," in *IECON 2019 - 45th Annual Conference of the IEEE Industrial Electronics Society*, 2019, vol. 1, pp. 2501–2506.
- [65] F. Mohammadzadeh Shahir and E. Babaei, "Application of high output voltage dc-dc converters along with using battery to extract maximum power from the solar cell," in *2017 8th Power Electronics, Drive Systems Technologies Conference (PEDSTC)*, Feb 2017, pp. 43–48.
- [66] Fei Xue, R. Yu, W. Yu, A. Q. Huang, and Yu Du, "A novel bi-directional dc-dc converter for distributed energy storage device," in *2015 IEEE Applied Power Electronics Conference and Exposition (APEC)*, March 2015, pp. 1126–1130.
- [67] J. Neely, S. Pekarek, R. DeCarlo, and N. Vaks, "Real-time hybrid model predictive control of a boost converter with constant power load," in *2010 Twenty-Fifth Annual IEEE Applied Power Electronics Conference and Exposition (APEC)*, 2010, pp. 480–490.

- [68] A. P. N. Tahim, D. J. Pagano, and E. Ponce, “Nonlinear control of dc-dc bidirectional converters in stand-alone dc microgrids,” in *2012 IEEE 51st IEEE Conference on Decision and Control (CDC)*, 2012, pp. 3068–3073.
- [69] J. Zeng, Z. Zhang, and W. Qiao, “An interconnection and damping assignment passivity-based controller for a dc-dc boost converter with a constant power load,” *IEEE Transactions on Industry Applications*, vol. 50, no. 4, pp. 2314–2322, 2014.
- [70] Tareq Alnejaili, Said Drid, Driss Mehdi, Larbi Chrifi-Alaoui, Rafik Belarbi, and Aziz Hamdouni, “Dynamic control and advanced load management of a stand-alone hybrid renewable power system for remote housing,” *Energy Conversion and Management*, vol. 105, pp. 377 – 392, 2015.
- [71] M. Cupelli, M. Mirz, and A. Monti, “Application of backstepping to mvdc ship power systems with constant power loads,” in *2015 International Conference on Electrical Systems for Aircraft, Railway, Ship Propulsion and Road Vehicles (ESARS)*, 2015, pp. 1–6.
- [72] Q. Xu, C. Zhang, C. Wen, and P. Wang, “A novel composite nonlinear controller for stabilization of constant power load in dc microgrid,” *IEEE Transactions on Smart Grid*, vol. 10, no. 1, pp. 752–761, 2019.
- [73] T. K. Roy and M. A. Mahmud, “Dynamic stability analysis of hybrid islanded dc microgrids using a nonlinear backstepping approach,” *IEEE Systems Journal*, vol. 12, no. 4, pp. 3120–3130, 2018.
- [74] M. M. Garg, Y. V. Hote, and M. K. Pathak, “Leverrier’s algorithm based modeling of higher-order dc-dc converters,” in *2012 IEEE 5th India International Conference on Power Electronics (IICPE)*, 2012, pp. 1–6.
- [75] A. Iovine, S. B. Siad, G. Damm, E. De Santis, and M. D. Di Benedetto, “Nonlinear control of a dc microgrid for the integration of photovoltaic panels,” *IEEE Transactions on Automation Science and Engineering*, vol. 14, no. 2, pp. 524–535, 2017.
- [76] R. Mahmud, M. A. Hossain, and H. Pota, “Robust nonlinear controller design for islanded photovoltaic system with battery energy storage,” in *2020 IEEE International Conference on Power Electronics, Smart Grid and Renewable Energy (PESGRE2020)*, 2020, pp. 1–6.
- [77] S. Shukla and B. Singh, “Reduced-sensor-based pv array-fed direct torque control induction motor drive for water pumping,” *IEEE Transactions on Power Electronics*, vol. 34, no. 6, pp. 5400–5415, 2019.

- [78] M. Satapathy, M. P. Korukonda, A. Hussain, and L. Behera, “A direct perturbation based sensor-free mppt with dc bus voltage control for a standalone dc microgrid,” in *2019 IEEE PES Innovative Smart Grid Technologies Europe (ISGT-Europe)*, 2019, pp. 1–5.

Index

- Back-stepping, 33
- Direct Perturbation MPPT, 18
- Disturbance Observer
 - Back-stepping Design, 40
- Estimation, 5
- Hierarchical Control, 30
- IntroMGStandalone, 18
- Irradiance Detection, 10
- Lyapunov Stability, 28
- Model-based MPPT, 5
- MPPT
 - Maximum Power Point Tracking, 5
- Newton-Raphson, 11
- Nonlinear Controller, 28
- PV Model, 7
- Secondary Control, 32
- Sensorless, 5, 21
- Single Step MPPT, 7
- SPVDG
 - Standalone Photovoltaic Distributed
 - Generation, 2
- SSA
 - State Space Averaging, 30
- Strict feedback, 28
- Temperature Detection, 10
- Unified Algorithm, 19